DETECTING MOISTURE IN BAUXITE USING MICROWAVES

LATA I. PAEA [1], SIONE PAEA [1] and MARK J. MCGUINNESS [2]

Abstract

Mathematical modelling of microwaves travelling through bauxite ore provides a way to compute moisture content in the free space transmission method given data on signal attenuation, phase shift and variable bauxite depth. We extend a recently developed four-layer model that uses coupled ordinary differential wave equations for the electric field together with continuity boundary conditions at interfaces between ore, air and antenna to find a solution that incorporates multiple internal reflections in ore and air. The model provides good fits to data, depending on ore permittivity and conductivity. Our extensions are to use effective medium models to obtain electromagnetic properties of the ore mixture from moisture content and to incorporate the damping effects of scattering from the ore surface. Our model leads to a formula for the received signal showing how signal strengths SS and phase shifts depend on the moisture content of the bauxite ore, through the effects of moisture on permittivity and conductivity. We show that SS may be noninvertible, indicating that attenuation data alone cannot be used to infer moisture content. Combining with phase data typically corrects the noninvertibility. Reducing the operating frequency dramatically improves the usefulness of signal strength data for inferring moisture content.

1. Introduction

The motivation for our modelling comes from a European Study Group with Industry held in 2017 at the University of Limerick. Electromagnetic measurements made by an automatic microwave analyser during offload of bauxite ore from a ship to an alumina factory were provided to the study group. Signal attenuation data indicated a highly nonlinear dependence on bauxite depth or height h, at odds with the linear calibration used in the microwave analyser to infer moisture content [23].

---

[1]School of Information Technology, Engineering, Mathematics and Physics, The University of the South Pacific, Suva, Fiji; e-mail: latapaea@gmail.com, sione.paea@usp.ac.fj
[2]School of Mathematics and Statistics, Victoria University of Wellington, Wellington, New Zealand; e-mail: Mark.McGuinness@vuw.ac.nz
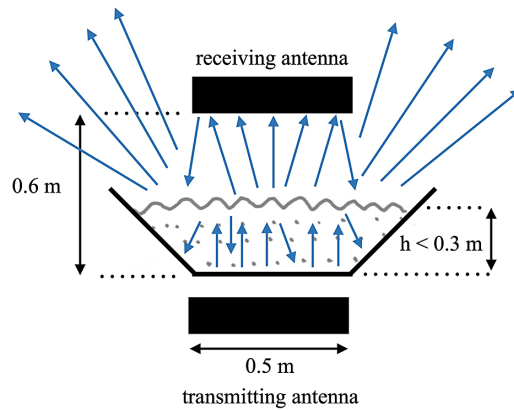
FIGURE 1. A sketch of the microwave analyser antennae mounted across a bauxite ore conveyor belt, showing key dimensions. The blue arrows illustrate microwave rays scattering from the rough ore surface, with some being lost to the environment. The ore is travelling into the page. (Colour available online.)

The alumina company has a strong interest in accurately measuring moisture content in bauxite ore, because payment for ore is by the tonne and the moisture content has a strong effect on the weight of the ore mix. So it is desirable to reliably and automatically check the moisture content. Spot checks on samples have traditionally been made and are a gold standard approach, being based on changes in mass measured in the lab after driving off the water content of a sample by heating. However, this process is labour-intensive and cannot be undertaken very frequently. Water has a relatively high permittivity for microwaves, so using a low-power microwave analyser to detect moisture content in a way that is nondestructive and almost continuous in time is a promising approach.

The microwave analyser is mounted across a conveyor belt that is transporting bauxite ore from ship to factory, with a square-shaped transmitting antenna close below the belt and an identical receiving antenna approximately 0.6 m above, arranged so that transmitted signals pass through the ore mixture before arriving at the receiving antenna, as sketched in Figure 1. This is termed the free space transmission method, especially when used to determine dielectric properties [8], although our purpose here is rather to measure moisture content.

The analyser measures raw electromagnetic microwave signal data, and a separately mounted ultrasound system simultaneously detects the height of bauxite currently on the belt. Measurements are made while the ore is moving on the conveyor belt at 1.8 m s^{-1}. Movement of the microwaves is to a good approximation one-dimensional and vertical. The ore is at varying heights but typically approximately 250 mm high and is approximately level on the top. However, the top is not smooth and has lumps of ore of varying size there. Once each second, the analyser outputs a moisture content M (wet basis, that is, the mass of water in a sample divided by the total mass of that sample of moist bauxite mixture). The algorithm used by the analyser to infer M is

$$M = c_0 + c_1 \frac{\Delta\phi}{h} + c_2 \frac{L}{h}, \tag{1.1}$$

where the constants c_0, c_1 and c_2 are fitted during calibration to the moisture content of laboratory samples, $\Delta\phi$ is the phase shift in radians in the complex valued electric field signal $E(h)$ at the receiving antenna when bauxite height is h and L is the signal attenuation, given in dB by

$$L = -20 \log_{10} \left| \frac{E(h)}{E(0)} \right|. \tag{1.2}$$

This form for attenuation is also referred to as the electromagnetic shielding efficiency [37] of the bauxite material. The phase shift (from the phase value of the detected electric field when $h = 0$) is the argument of the complex number $E(h)/E(0)$,

$$\Delta\phi = \arg\left(\frac{E(h)}{E(0)} \right).$$

This is similar to the approach reported by Vianna [36] for a microwave analyser in an alumina factory in Brazil. They had access to belt tonnage measurements, but they reported more reliable results if they used measurements of material height, thereby assuming (as we do here) constant material porosity.

The raw data measured by the microwave analyser are signal strength ($-L$) and two phase shifts. The scales for this data are arbitrary, calibrated when setting up the analyser to be a number in the range [0,1000]. The two phase values, together with ore height values, may be interpreted, as explained by [23], to obtain the lifted or total phase shift of the microwave signal $\Delta\phi$ in radians, zeroed at $h = 0$. One phase shift of the received signal relative to a reference signal is usually computed in electronic equipment by clipping each signal to a square wave with amplitude in the set {0,1}, then taking the average area of the XOR of the waves over some time that is much larger than their period. This provides a number θ for the phase difference in the range [0, π] for a signal expressed using radians as (say) $\sin\theta$. A second phase shift is obtained by shifting the first by approximately $\pi/2$, so that together, they can be used to provide a phase shift in the range [0, 2π]. The phase shift range can be extended indefinitely [23] beyond [0, 2π] by also using the height data that are simultaneously collected by an ultrasound system attached to the microwave analyser.

The linear dependence on bauxite height h used in the calibration (1.1) is a poor fit to signal strength data [23, 25]. A linear behaviour is consistent with semi-infinite models that ignore reflections in ore and air layers, whereas data indicate that attenuation is dominated by the nonlinear interference effects associated with reflections that depend strongly on a variable bauxite ore height h. Hence, the linear regression that is routinely used in automated microwave analysers may fail to accurately infer moisture content from signal strength, when the range of ore heights or ore wetness gives a strongly nonlinear dependence on h.

The four-layer model developed by Paea et al. [25] provides a better match to nonlinear attenuation data and notes the important effects of signal reflections on that

data. There is some exploration of the effects of mixture electromagnetic properties on data. However, there is no consideration in [25] of how to determine moisture content using the four-layer model.

Our primary motivation here is to use mixture theory to connect moisture content to average electromagnetic properties, especially permittivity and electric conductivity, allowing the use of the four-layer model to predict moisture content from phase shift and attenuation data. This would be considered as an improvement in the usefulness of the four-layer model in the industrial context, where the interest is in inferring moisture content from analyser data. It also improves the accuracy of the model by explicitly allowing for the fact that variations of moisture content affect both permittivity and conductivity, so that these two parameters are not really independent as assumed by Paea et al. [25].

A concerning result in that paper [25] is that data are not always invertible when inferring electromagnetic properties, particularly when inferring mixture permittivity solely from strength data. This raises an important question as to whether the same issue of noninvertibility applies to inferring moisture content from data when using the four-layer model. So while our primary motivation in linking moisture to electromagnetic properties is to be useful to users of the microwave analyser, such a link will allow us also to answer the question: is it mathematically possible to infer moisture content from data according to the mathematical model solution?

A second motivation and point of difference for the present work is that we seek to improve the four-layer model by extending it to allow for the effects of scattering at the rough upper surface of the bauxite ore.

We summarise in Section 2 the four-layer model and solution of Paea et al. [25], then in Section 3, we review the existing relationships between ore electromagnetic properties, and its porosity and moisture content, which allow us to provide preliminary results on the use of a microwave analyser for inferring moisture content of bauxite ore in real time.

In Section 4, we extend the four-layer model to allow for the effects of scattering in the region above the bauxite. Our extended model is solved to provide an explicit forward formula for the received signal when microwaves pass through bauxite ore and scatter in the air space above it. This formula depends on the operating frequency of the microwaves, antenna properties, the amount of scattering above the bauxite, the permittivity of solid ore, the porosity of the mined ore mixture, the electrical conductivity of the liquid in the pores and the moisture content of the ore. The extended model is compared in Section 5 with our previous model, and the invertibility of our extended model is explored, together with its dependence on the key parameters of the bauxite and microwave system. Conclusions follow in Section 6.

2. Four-layer mathematical model

We begin with a description of the model published by Paea et al. [25], which provides good fits to analyser data. The four layers or regions in our conceptual and
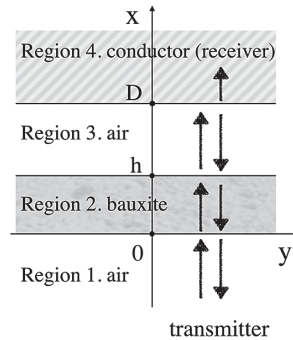
FIGURE 2. A sketch of the four-layer model, showing origin, and the distances D and h in the x-direction. Arrows indicate directions of travel for the plane electromagnetic waves.

mathematical model (a layer of bauxite ore sandwiched between two air layers, with a conducting antenna or receiver on the top) are sketched in Figure 2 together with directions of travel for the plane wave solutions, approximated at this stage as being in the vertical dimension. We do not explicitly model the transmitting antenna.

The origin of the model is fixed at the surface of the empty conveyor belt. The variable nonnegative bauxite height is denoted h, while the receiving antenna is fixed at $x = D > h$. The wave arriving at the base of the bauxite from the transmitting antenna is taken to be a free space wave travelling in the positive x-direction, with axes oriented so that the electric field has z-component $E(x)e^{-i\omega t}$ and the magnetic field has y-component $H(x)e^{-i\omega t}$. The angular frequency is $\omega = 2\pi f$ and the operating frequency f is listed in Table 1 for the data we use. It is a consequence of Maxwell's equations that electric fields $E(x)$ in all layers then satisfy the wave equation, which is a linear differential equation,

$$\frac{\partial^2 E}{\partial x^2} = -\mu\omega^2\epsilon E - i\mu\omega\sigma E, \tag{2.1}$$

where $i^2 = -1$. The permittivity ϵ and the electrical conductivity σ take different values in different layers, while the permeability is taken to be that of free space $\mu = \mu_0$ in all four layers, since bauxite ore is usually considered to be nonmagnetic [25]. Parameter values used later, unless noted otherwise, are listed in Table 1.

Without loss of generality, we take permittivity ϵ and conductivity σ to be real quantities. The permittivity is $\epsilon = \epsilon_r\epsilon_0$, where relative permittivities ϵ_r take the value one in air and antenna. The relative permittivity of the bauxite ore mixture depends strongly on moisture content, because water has a high value of relative permittivity compared with dry solid bauxite. Electrical conductivity σ is zero in air and negligible in solid bauxite, and is high in the receiving antenna. It is also an important property in the bauxite mixture that varies with moisture content, because pore water is expected to contain significant dissolved salts.

TABLE 1. Model parameters and default values used in four-layer model simulations.

Parameter	Value	Units	Comment
D_0	0.615	m	estimated from scale drawings & fitting
f	0.9	GHz	microwave frequency
h_m	0.2	m	sag midpoint
k_s	1.5	m^{-1}	scattering damping
M	0.1	mass fraction	moisture content
n	0.42	volume fraction	porosity
S_e	0.1	m	sag extent
S_m	0.04	m	max sag amplitude
ϵ_0	8.85×10^{-12}	F.m^{-1}	free space permittivity
ϵ_{rA}	1		antenna relative ϵ
ϵ_{rb}	6		solid ore relative ϵ
ϵ_{rw}	80		water relative ϵ
μ_0	$4\pi \times 10^{-7}$	H.m^{-1}	free space permeability
ρ_a	1.2	kg.m^{-3}	density of air
ρ_s	2800	kg.m^{-3}	density of solid
ρ_w	1000	kg.m^{-3}	density of water
σ_A	50	S.m^{-1}	antenna conductivity
σ_b	40	mS.m^{-1}	ore mixture conductivity
σ_w	1.2	S.m^{-1}	water conductivity

The substitution of $E = e^{ikx}$ into (2.1) gives a quadratic for wavenumber k,

$$k^2 = \omega^2 \epsilon \mu (1 + i \mathcal{D}), \tag{2.2}$$

where the dissipation $\mathcal{D} = \sigma/(\omega\epsilon)$ is the magnitude of the conduction current density divided by the magnitude of the displacement current density [22], and is zero in air. Then there are two solutions $\pm k$, complex-valued in bauxite and in the receiving antenna, but real-valued in air:

$$k = \Re(k) + i\Im(k).$$

The real part of k may be written in the form [22, 11.3.1]

$$\Re(k) = \omega\sqrt{\frac{\epsilon\mu}{2}}(\sqrt{1 + \mathcal{D}^2} + 1)^{1/2},$$

while the imaginary part of k may be written in the form

$$\Im(k) = \omega\sqrt{\frac{\epsilon\mu}{2}}(\sqrt{1 + \mathcal{D}^2} - 1)^{1/2}.$$

The real part of k gives the wavelength $\lambda = 2\pi/\mathfrak{R}(k)$ of electric field oscillations. The imaginary part gives growth or decay rates of the amplitudes of these oscillations as x increases.

2.1. Model solutions   The solutions to the differential equations in each layer take the general form

$$E = E_+ e^{ikx} + E_- e^{-ikx}. \tag{2.3}$$

Each part of the solution (2.3), when considered together with the time dependence $e^{-i\omega t}$, corresponds to a wave that travels in the positive or negative x-direction, respectively. We seek the solution at the surface $x = D$ of the receiving antenna, the upward-travelling wave

$$E_a = E_{4+} e^{ik_A(x-D)} = E_{4+}.$$

Solving our coupled system of differential equations is possible, determining at the same time all reflection and transmission coefficients, thanks to the boundary conditions that arise from requiring continuity of electric and magnetic fields tangential at each interface in the model. The details are given in detail in [25] and are summarised in Appendix A for completeness. The solution is

$$E_a = E_{4+} = \frac{8Z_0^2 Z_A Z_b \, e^{ik(D-h)} e^{ik_b h}}{F}, \tag{2.4}$$

where

$$\begin{aligned} F = &(Z_b^2 - Z_0^2)(Z_0 - Z_A)(e^{2ik_b h} - 1)e^{2ik(D-h)} \\ &+ [(Z_0 - Z_b)^2 e^{2ik_b h} - (Z_0 + Z_b)^2](Z_0 + Z_A), \end{aligned}$$

and the impedance of material with subscript $i = 0, A, b$ (free space, antenna and bauxite ore) is $Z_i = \mu_i \omega / k_i$. Elsewhere, the subscript b indicates properties of the bauxite ore mixture and the subscript A indicates effective properties in the receiving antenna region. The symbol k with no subscript is used for the wavenumber in air, where the dissipation $\mathcal{D}$ is zero and k is real.

Equation (2.4) looks complicated, but the exponential terms indicate the major dependence on $k(D - h)$, due to the air layer in Region 3 of thickness $D - h$ with no attenuation, and on $k_b h$, due to the bauxite layer in Region 2 of thickness h with some attenuation. In particular, the wavelengths of the resulting received signal can be seen to be determined by the sums and differences of the real part of k_b and k. Bauxite mixture properties affect the values of ϵ_b and σ_b, which directly affect k_b and Z_b according to (A.1).

Previous work [25] has shown that the four-layer solution (2.4) has behaviour that is a good match to attenuation data obtained from an alumina manufacturer in Ireland. A typical set of matches of our model solution to attenuation and phase data is presented here in Figure 3 for two different values for the effective relative permittivity
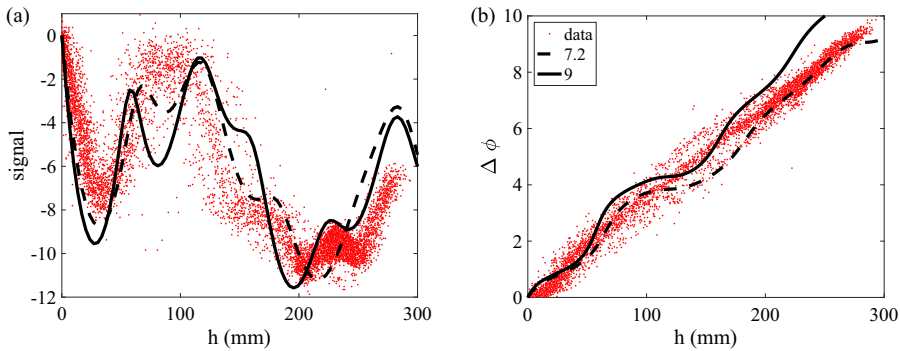
FIGURE 3. Model solutions (lines) compared with data (dot symbols) obtained with a microwave analyser. The data are signal strength and phase shift $\Delta\phi$ (radians) at the receiving antenna, plotted against ore height h. Signal strength data have been linearly scaled to provide a visual match to the model results, which are in dB. The relative permittivities of the bauxite ore mixture used for the two model solutions are listed in the legend. Sag is set to zero here. Other parameter values are listed in Table 1.

ϵ_r of the bauxite mixture. In particular, the wavelengths associated with reflections and interference in the air gap Region 3 above the bauxite, and the shorter wavelengths arising from reflections within the bauxite ore, are apparent in the attenuation data and, to a lesser extent, in the phase shift data.

3. Moisture in ore

The outstanding question is the one originally posed by the alumina manufacturer at the European Study Group with Industry at the University of Limerick in 2017, that is, how to use the microwave analyser data to accurately infer moisture content in the bauxite ore. The four-layer model [25] provides good matches to analyser data and explains what is causing the oscillations seen especially in attenuation, but it only allows to infer electromagnetic properties of the ore mixture and stops short of using data to infer the moisture content of the ore.

We briefly review theories of how the relative amounts of components of a mixture of solid bauxite, air and water affect the measured average or effective values of permittivity and conductivity of the bulk mixture. We adopt soil and porous medium conventions for describing the mixture. The ore is considered to be a solid with porosity n, and the pore space is occupied by air and water. The term solid is used to refer to all of the components in the mix that are not air or liquid water, irrespective of their state. The liquid saturation S is the volume fraction of pore space occupied by liquid water. Air then occupies the remaining volume fraction $1 - S$ of pore space. Saturation ranges from zero to one in value and, together with porosity and densities, determines the water fraction by weight. Solid ore occupies the volume fraction $(1 - n)$. We seek averaged or effective properties of the ore as a conducting dielectric mixture, when high-frequency EM waves pass through at frequencies above 100 MHz.
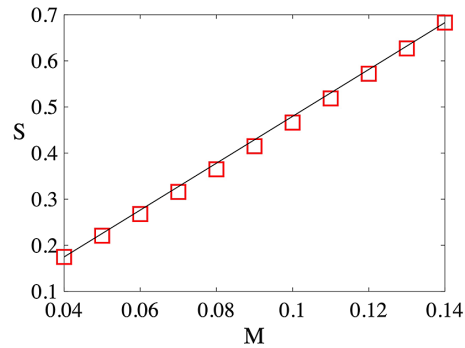
FIGURE 4. Liquid water saturation S as a function of water content M (mass %, wet basis) (symbols). The straight solid line joins the first and last data points to illustrate linearity. Parameter values used are as listed in Table 1.

The relative permittivity of the solid matrix that characterises the dry bauxite parent matrix is variable and is sensitive to clay content, but it remains much less that the value for water. Schön [28, Section 8.7.2] lists values for smectite, kaolin, illite and quartz in the range $4 \leq \epsilon_{rb} \leq 10$, with lower values for frequencies near 1 GHz. Anecdotally, there are four different types of bauxite shipped into the factory near Limerick, which may have four different values for solid permittivity. The water content is known to have a strong influence on the mixture permittivity ϵ_r. The solid permittivity is an unknown parameter that needs to be determined by calibration or directly measured before using a microwave analyser to infer moisture content.

The moisture content M as a mass fraction on a wet basis is the mass of water in a given mass of mixture,

$$M = \frac{nS\rho_w}{nS\rho_w + (1-n)\rho_s + n(1-S)\rho_a},$$

with parameter values given in Table 1. Rearranging this definition gives the saturation S as a function of M for given n and density values,

$$S = \frac{M[(1-n)\rho_s + n\rho_a]}{n[\rho_w(1-M) + \rho_a]}. \tag{3.1}$$

A plot of saturation S versus moisture content M over the moisture range $[0.04, 0.14]$ will be nearly linear since $1 - M \approx 1$. The plots in Figure 4 for porosity $n = 0.5$ illustrate how linear $S(M)$ is, as well as the typical ranges of S resulting from the usual ranges of moisture content seen in bauxite ore shipments.

The laboratory measurements that are used in the bauxite industry to independently measure water content and then to calibrate the microwave analyser are based on weights measured before and after heating the bauxite samples in an oven. Heating

to 100°C may not drive off tightly bound water [39]. Heating to 200°C is usually enough to drive off most of the bound water. Bound water content can be up to 4% by weight if organic matter is not present, depending on the specific surface area of the soil (especially the clay content); typically, approximately 20% of bound water is tightly bound.

Connolly et al. [6] note that at frequencies above 10 MHz, the dielectric permittivity of reservoir rocks containing water and oil relates primarily to the volume fractions of constituent minerals and saturation, and is not sensitive to the distinction between bound and free water. At low frequencies below 10 MHz, bound water is associated with interfacial polarisation, electro-diffusion and ohmic conduction, which have an affect on measurements. Hence, for our purposes, the distinction between bound and free water is not relevant as the frequencies under consideration are above 10 MHz.

The mining and loading process means that an approximation of the bauxite ore mixture as a random mixture of solid, air and liquid is likely a good one. The bauxite offloaded from a ship has been mined from natural rock formations which, before mining, have a wide range of porosities. It contains a range of particle sizes and looks like lumpy soil. It typically consists of a reddish clay material, containing hydrated alumina with variable proportions of iron oxides, silica and titanium dioxide. The space available to be filled with water inside the bauxite is the porosity n, a volume fraction. Porosity takes values ranging from 0.41 to 0.67 for loams and sands [27]. Polydisperse sands [24] have $n \in [0.30, 0.35]$. Guelph silt loam [33] has $n \in [0.4, 0.5]$. Bulk density of bauxite is typically 1400–1500 kg m^{-3}. If rock density is 2800 kg m^{-3}, this implies a porosity of value 0.5.

We will use the notation

$$\epsilon = \epsilon_r \epsilon_0, \quad \epsilon_b = \epsilon_{rb} \epsilon_0, \quad \epsilon_a = \epsilon_{ra} \epsilon_0, \quad \epsilon_w = \epsilon_{rw} \epsilon_0$$

for relative permittivities of mixture, bauxite solids, air and water, respectively.

3.1. Mixture permittivity Reviews of studies of the macroscopic dielectric properties in the geophysical and physics contexts include [3, 21, 31, 32, 34]. Early work on how the properties of mixtures depend on the properties of constituents goes right back to Maxwell in 1864 and the Clausius–Mossotti relation [22, Section 3.8] for the effective relative permittivity ϵ_r when there are N_j molecules of species j present in a unit volume of free space, each with polarisability α_j:

$$\frac{\epsilon_r - 1}{\epsilon_r + 2} = \frac{1}{3\epsilon_0} \sum_j N_j \alpha_j.$$

L.V. Lorenz and H.A. Lorentz obtained a similar formula for refractive index [31, Ch. 1].

In 1892, Lord Rayleigh used the Clausius–Mossotti relation to calculate the Rayleigh mixing formula for the effective relative permittivity ϵ_r of a mixture with spherical or cylindrical inclusions ordered in a rectangular matrix. It generalises for K

different types of inclusion in free space to [31, Section 4.1]

$$\frac{\epsilon_r - 1}{\epsilon_r + 2} = \sum_{j=1}^{K} f_j \left(\frac{\epsilon_j - 1}{\epsilon_j + 2} \right),$$
(3.2)

where f_j is the volume fraction occupied by the jth type of inclusion which has relative permittivity ϵ_j.

The Rayleigh mixing formula is also known as the Maxwell–Garnett mixing rule [31, 32] and is related to work by Wagner in 1924 [3], when made explicit in the effective permittivity.

This early work was derived in the limit of very dilute mixtures and was found to give poor matches to experimental measurements. A response with good matches to data has been termed the Maxwell–Wagner–Bruggeman–Hanai (MWBH) theory of effective media [2, 5, 12]. Bruggeman developed new theories which do not require dilute mixtures, which take account of bulk properties, shape and volume fractions of components. The MWBH theory has been found to correctly predict both the permittivity and the conductivity for porous water-bearing rocks at frequencies greater than 10 MHz [3, 4]. At lower frequencies, surface effects associated with bound water can render the MWBH theory ineffective in matching experimental data. The frequencies in which we are interested allow us to use the MWBH theory, which depends on bulk or total water content.

Bruggeman developed two major formulae, one symmetric and one nonsymmetric, for a single inclusion in a parent material. In terms of a parent material that is solid bauxite, with water included via a saturated porosity n, Bruggeman's symmetric mixing formula is

$$n \left(\frac{\epsilon_{rw} - \epsilon_r}{\epsilon_{rw} + 2\epsilon_r} \right) + (1 - n) \left(\frac{\epsilon_{rb} - \epsilon_r}{\epsilon_{rb} + 2\epsilon_r} \right) = 0.$$
(3.3)

The effective relative permittivity ϵ_r of the mixture is given implicitly by (3.3). The same result can be derived using a self-consistency argument in the effective medium approach [1, 19, 20, 34].

The symmetric formula (3.3) can be written as a quadratic in the permittivity ϵ_r of the averaged medium. The correct root may be chosen by noting that there are bounds on its value, corresponding to parallel and series circuits [16], also termed Weiner's upper and lower bounds [16]. Alternatively, the correct root follows by ensuring one chooses the root with the correct limiting values as n goes to zero or one. A simple approach is to express n as a function of ϵ_r, then switch x- and y-axes. Porosity does not have to be small in (3.3). Relatively modern derivations of Bruggeman's symmetric equation (3.3) use effective medium approximations [1, 19, 34].

Using his symmetric form, Bruggeman developed and solved a differential equation, obtaining a nonsymmetric form for permittivity as a function of volume fraction
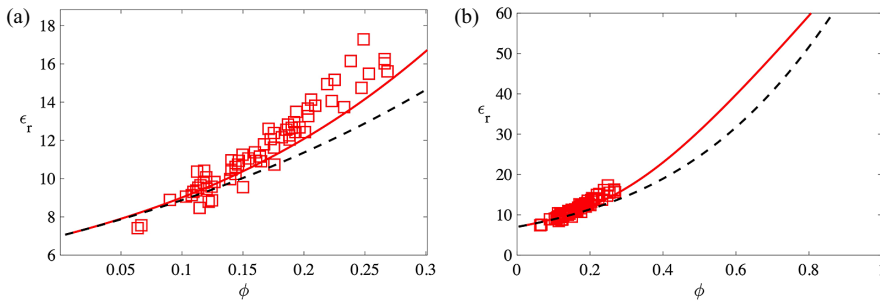
FIGURE 5. Comparisons of measured permittivity in saturated sandstones (symbols) with Bruggeman's nonsymmetric formula (3.4) (the MWBH formula, dashed line) and his symmetric mixing formula (3.3) (solid line). Measured data are at frequency 0.5 GHz in saturated tight gas sandstones [7]. A dry bauxite permittivity $\epsilon_b = 7$ has been used for the theoretical formulae.

of contaminant,

$$\left(\frac{\epsilon_{rw} - \epsilon_r}{\epsilon_{rw} - \epsilon_{rb}}\right)\left(\frac{\epsilon_{rb}}{\epsilon_r}\right)^{1/3} = 1 - n. \tag{3.4}$$

Some authors [3, 5] refer to this nonsymmetric Bruggeman solution (3.4) as the MWBH solution. Hanai [11] showed that both Bruggeman formulae can be generalised to electrical conductivities or complex-valued permittivities. Hanai et al. [10, 12, 13] find that the nonsymmetric Bruggeman solution (3.4) is a good match to measurements of dielectric permittivity, and of electrical conductivity in water and oil emulsions.

Comparisons of Bruggeman's nonsymmetric formula (3.4) and symmetric formula (3.3) with data from saturated sandstone in Figure 5 suggest that both formulae give reasonable matches.

Pecharroman and Iglesias [26] note that Landauer [20] has also obtained Bruggeman's symmetric formula, which is easily extended to cases with more than one inclusion [21]. It seems that Landauer was at first unaware of Bruggeman's results [9] from 1935.

The Bruggeman nonsymmetric formula is for a single inclusion (water) in solid bauxite. A very interesting extension to this model, which allows for two inclusions (water and air) in solid bauxite, is provided by Jayannavar and Kumar [17]. They begin with Bruggeman's symmetric mixing formula (3.3) which becomes the following for our mixture of solid bauxite, air and water:

$$nS\left(\frac{\epsilon_{rw} - \epsilon_r}{\epsilon_{rw} + 2\epsilon_r}\right) + n(1 - S)\left(\frac{\epsilon_{ra} - \epsilon_r}{\epsilon_{ra} + 2\epsilon_r}\right) + (1 - n)\left(\frac{\epsilon_{rb} - \epsilon_r}{\epsilon_{rb} + 2\epsilon_r}\right) = 0,$$

where ϵ_r is the effective relative permittivity of the mixture. They point out that the unsymmetrical Bruggeman formula is more appropriate to physical situations like saturated porous media, where the background solid phase is not on an equal footing with the filling phase. The symmetrical formula is more suited to ideal binary systems where the two phases should be treated on an equal basis. In seeking a unified

treatment of the symmetrical and unsymmetrical formulae, Jayannavar and Kumar use a renormalisation procedure very much like Bruggeman's derivation that provides an effective medium for a ternary system, like our present case of a solid bauxite porous medium with porosity occupied by air and water. They find a unified solution for the effective relative permittivity ϵ_r of the mixture that is given in our notation by

$$\left|\frac{\epsilon_+ - \epsilon_r}{\epsilon_+ - \epsilon_{rb}}\right|^B \left|\frac{\epsilon_- - \epsilon_r}{\epsilon_- - \epsilon_{rb}}\right|^C \left(\frac{\epsilon_{rb}}{\epsilon_r}\right)^{1/3} = 1 - n, \tag{3.5}$$

where

$$\begin{aligned} B &= \frac{(\epsilon_{rw} + 2\epsilon_+)(\epsilon_{ra} + 2\epsilon_+)}{6\epsilon_+(\epsilon_+ - \epsilon_-)}, \\ C &= \frac{(\epsilon_{rw} + 2\epsilon_-)(\epsilon_{ra} + 2\epsilon_-)}{6\epsilon_-(\epsilon_- - \epsilon_+)}, \end{aligned} \tag{3.6}$$

and $\epsilon_\pm$ are the roots of the quadratic in ϵ,

$$S(\epsilon_{rw} - \epsilon)(\epsilon_{ra} + 2\epsilon) + (1 - S)(\epsilon_{ra} - \epsilon)(\epsilon_{rw} + 2\epsilon) = 0. \tag{3.7}$$

The power of 1/3 follows from inserting the air permittivity value $\epsilon_{ra} = 1$. This specialises (3.5) to apply to relative permittivity; using absolute permittivities is also possible using the same formula.

The unified solution (3.5) of Jayannavar and Kumar extends Bruggeman's non-symmetric solution to the case to two inclusions, and implicitly gives the relative permittivity of a mixture of bauxite, liquid water and air, where solid bauxite has porosity n and the liquid saturation is S in the pores. This provides the connection we need between porosity, saturation and permittivity of bauxite ore. It is symmetrical with respect to interchanging air and water.

As Jayannavar and Kumar point out, their solution provides a unification of Bruggeman's very successful formulae, symmetrical and nonsymmetrical. If we let $S \to 0$ or $S \to 1$, then we find that $C \to 0$ and $B \to 1$, and the original MWBH (nonsymmetrical) formula for one contaminant (air or water, respectively) is recovered. If we set the permittivity of air to match that for water, we also recover the MWBH nonsymmetrical formula. However, if we set porosity to one, we recover the symmetrical Bruggeman formula for air and water in free space (because then, $\epsilon_r = \epsilon_+$ or $\epsilon_r = \epsilon_-$ and the quadratic (3.7) is the symmetrical formula).

The permittivities in the above may be absolute permittivity or relative permittivity. When real permittivities are used, as in our development, there are always two different real roots of the quadratic (3.7).

Then given bauxite porosity n and the moisture content by mass fraction M, (3.1) gives liquid volume saturation S, and (3.7) gives the quadratic whose roots $\epsilon_\pm$ are needed. The roots can be found numerically or by using the quadratic formula. Then the terms B and C in (3.6) can be calculated, and (3.5) can be solved implicitly to find the relative permittivity ϵ_r of the mixture of bauxite, water and air. This provides for
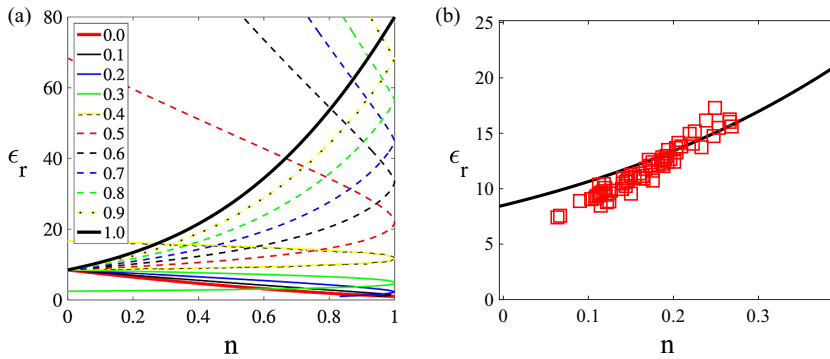
FIGURE 6. Solutions (3.5) obtained by calculating porosity n for given average relative permittivity of a mixture of bauxite, water and air, then switching abscissa and ordinate axes to get permittivity as a function of n. In panel (a), each curve is for a different value of saturation S as shown in the legend. Each curve doubles back at $n = 1$ and is multiple-valued, requiring care when the inverse function is sought. In panel (b), the saturated case $S = 1$ (solid line) is compared with saturated sandstone data [7] (symbols). The solid matrix relative permittivity has been set to 8.5 in both plots. (Colour available online.)

our model the connection between water content and the permittivity of the bauxite mixture.

The Jayannavar and Kumar unified solution has a critical value of saturation $S = S_c$ at which $\epsilon_+ = \epsilon_{rb}$. Then the solution (3.5) is undefined, and the correct solution is that the effective relative permittivity of the mixture is constant and is equal to ϵ_{rb}, independent of n. This is because at this value of saturation, the combination of water and air that is being added or subtracted as n varies has the same permittivity as the parent bauxite, so changing the porosity has no effect on permittivity.

One way to solve (3.5) explicitly is to make porosity n the subject, giving n explicitly in terms of ϵ_r and S. Then switch axes to obtain ϵ_r versus n at a given value of S, as illustrated in Figure 6 for $S = 1$.

For a given S, there are typically two branches of the solution formula (3.5) seen, joined at $n = 1$, when trying ϵ_r in the range $[1, \epsilon_{rw}]$. This is illustrated in Figure 6, where mixture relative permittivity ϵ_r is plotted against porosity n for several fixed values of saturation S and with solid bauxite relative permittivity set to $\epsilon_{rb} = 8.5$ for illustration purposes. It is important to choose the branch that comes out of the correct initial value $\epsilon_r(0) = \epsilon_{rb} = 8.5$, before doubling back at $n = 1$. For saturations above critical, this is the lower branch; for saturations below critical, the correct branch is the upper one, in a plot of $\epsilon_r(n)$.

We are interested in the effect of adding water to, or removing it from, bauxite, with a given fixed porosity. This means changing the saturation S for fixed n. Note that the branches join at $n = 1$, that is, when $\epsilon_r = \epsilon_+$, which is when
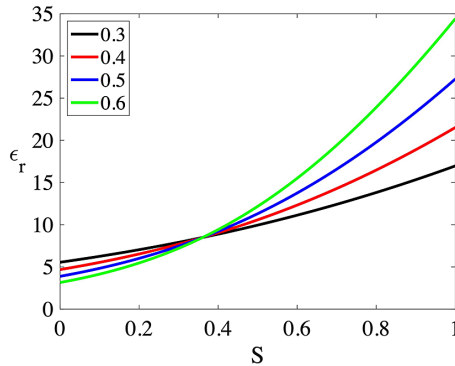
$$\epsilon_r = (-b + \sqrt{b^2 - 4ac})/(2a),$$

FIGURE 7. Solutions to (3.5) obtained by using an implicit equation solver (FZERO in MATLAB) on restricted ranges of mixture permittivity. Mixture permittivity is plotted against liquid water saturation, for porosity values $n = 0.3, 0.4, 0.5, 0.6$ as in the legend. Dry bauxite relative permittivity has been set to 8.5. (Colour available online.)

where a, b and c are the coefficients in the quadratic (3.7) for ϵ expressed in the popular form $a\epsilon^2 + b\epsilon + c = 0$, and

$$a = 2, \quad b = \epsilon_{ra}(3S - 2) + \epsilon_{rw}(1 - 3S), \quad c = -\epsilon_{ra}\epsilon_{rw}.$$

Note that the correct solution branches all have ϵ_r values that lie between dry bauxite ϵ_{rb} and the fully saturated solutions $\epsilon_r = \epsilon_+$. Hence, we ensure we are on the correct branch when solving implicitly, by restricting the search for the value of ϵ_r, given S, as follows:

(a) if $S < S_c$, the correct branch lies in $[\epsilon_+, \epsilon_{rb}]$;
(b) if $S = S_c$, the solution is $\epsilon_r = \epsilon_{rb}$;
(c) if $S > S_c$, the correct branch lies in $[\epsilon_{rb}, \epsilon_+]$.

The resulting values of mixture relative permittivity ϵ_r are plotted against liquid water saturation for $n \in [0.3, 0.6]$ in Figure 7, after setting $\epsilon_{rb} = 8.5$ for illustration purposes. Note the curves all pass through the critical value $S_c \approx 0.361$, where mixture permittivity matches dry bauxite permittivity.

A plot of inferred mixture relative permittivity, as a function of moisture content that is given by (3.5), is presented in Figure 8 for various porosity values and using dry bauxite permittivity $\epsilon_{rb} = 8.5$. Equation (3.1) is used to convert from moisture content M to saturation. We use (3.5) and (3.1) to connect bauxite mixture permittivity to moisture content in the remainder of this paper.

3.2. Bauxite conductivity   The Bruggeman approach outlined above may, in principle, be used to also calculate mixture conductivity. Equation (3.5) cannot be directly translated from permittivities to conductivities as, for example, the power of 1/3 is directly due to air having a relative permittivity of one. Using the Rayleigh mixing formula (3.2) or Bruggeman's symmetric formula (3.3) leads to a mixture conductivity
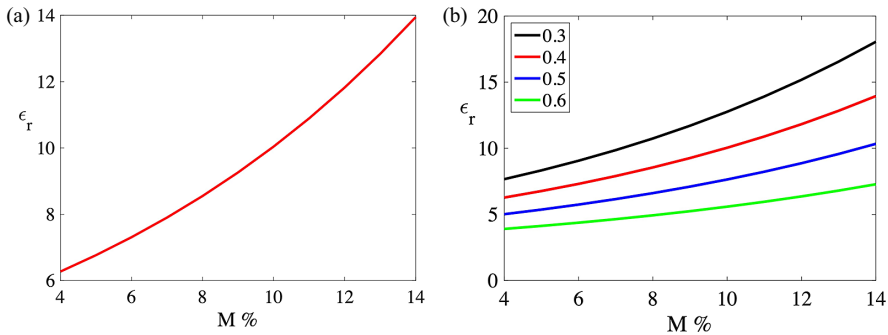
FIGURE 8. Mixture relative permittivity as a function of water content M (mass %, wet basis). Relative permittivity calculated using the extended nonsymmetric Bruggeman solution (3.5), with saturation given as the function (3.1) of water content M. Density values used are listed in Table 1. Porosity is set to 0.4 in panel (a) and to values in the range [0.3, 0.6] as indicated in the legend in panel (b). Solid dry bauxite relative permittivity has been set to 8.5 in all plots for illustration purposes. (Colour available online.)

that is linear in moisture content, whereas experiments indicate that a quadratic power law (Archie's law) is a more accurate fit [14, 15].

Measured values of conductivity for soils depend strongly on the clay component, partly because finer soils retain more moisture. Values for sands are $\sigma \in [0.1, 2]$ mS m^{-1}, for silts $\sigma \in [2, 20]$ mS m^{-1} and for clays $\sigma \in [10, 1000]$ mS m^{-1} [30]. Other measurements of dry and wet soils [29, 30] give electrical conductivity values in the range of 10–100 mS m^{-1}.

The electrical conductivity of air is zero and we expect that the electrical conductivity of perfectly dry solid bauxite is negligible, since feldspars have $\sigma \approx 10^{-11}$ S m^{-1}, and clays have $\sigma \approx 10^{-7}$ S m^{-1} [18]. Hence, our case is similar to that of a single conductor (brine) in free space. A simpler derivation of the equivalent to Bruggeman's nonsymmetric formula is then possible. Landauer [21], for example, finds that starting with pure conductor and removing portions of it, renormalising in the same spirit as Bruggeman, Archie's law can be derived giving the mixture conductivity as

$$\sigma = \sigma_0 \theta^{3/2},$$

with σ equal to the pure conductor value σ_0, when the volume fraction of pure conductor is $\theta = 1$.

Hunt et al. [14] find that electrical conductivity is better modelled for porous media in three dimensions by Archie's empirical law with power two, giving

$$\sigma = \sigma_w \theta^2, \tag{3.8}$$

where $\theta = nS$ is moisture content as a volume fraction and σ_w is related to the conductivity of the water in the pores. Hence, in this simple percolation model, σ starts at zero for completely dry bauxite and then increases with an increasing amount
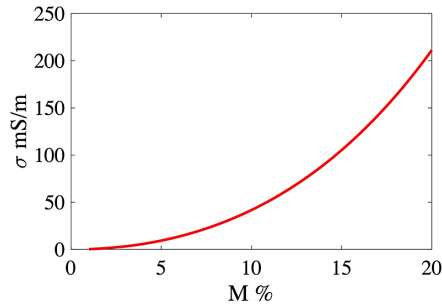
FIGURE 9. Mixture electrical conductivity σ as a function of water content M (mass %, wet basis). Electrical conductivity was calculated using the percolation model (3.8) with saturation given as the function (3.1) of water content M. Other parameter values are as listed in Table 1.

of water in pores. The behaviour (3.8) is a good match to numerous experiments on partially saturated soils [14, 15], so this is the model we will use here.

The pore water is in contact with salts in the solid bauxite and is also vulnerable to seawater entry during shipment to a factory. It is likely to contain ions, which can strongly increase its electrical conductivity. Seawater has surface conductivities σ_w that range from 2.5 to 5 S m^{-1} [35]. This provides an order of magnitude guide to the upper limit we might expect for σ_w. Calibrating our four-layer model to data from the Maia shipment of bauxite, where $\sigma = 40$ mS m^{-1} and lab moisture measurements are approximately $M = 10\%$, so that $S = 0.5$ and $\theta \approx 0.2$, suggests that the pore water in the ore has

$$\sigma_w \approx 1.2 \, \text{S/m}.$$

The resulting dependence of electrical conductivity for wet bauxite of porosity 0.4 on moisture content M is plotted in Figure 9.

3.3. Preliminary results   We now use in our four-layer model solution (2.4) the dependences of mixture permittivity and conductivity on moisture content summarised in (3.5) and (3.8), together with the relationship (3.1) between saturation S and moisture content M.

The four-layer model solution (2.4) then depends on a number of parameters that need to be determined by calibrating against data. They are D_0 (distance from empty belt to receiving antenna), ore porosity n, water conductivity σ_w, solid ore relative permittivity ϵ_{rb} and the main quantity that we are interested in determining from analyser data, moisture content M (mass fraction, wet basis). There is also a small dependence on belt sag.

Values that are used in the following sections (unless otherwise stated) are listed together with posited antenna values in Table 1. Salty pore water has almost the same relative permittivity as pure water, so we use $\epsilon_{rw} = 80$. The data used for comparison in the figures to follow have been obtained using a microwave analyser during offload of ore from the ship Maia.
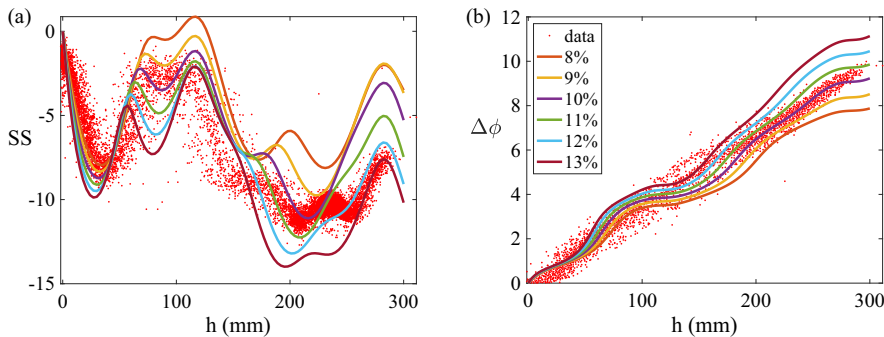
FIGURE 10. Four-layer model solutions (lines) compared with data (dot symbols) for various moisture content values. The data are signal strength SS (dB) and phase shift $\Delta\phi$ (radians) at the receiving antenna. The moisture contents used in the model are given in the legend. Other parameter values are listed in Table 1. There is no scattering or sag allowed for in this model. (Colour available online.)

Attempts to fit the four-layer solution to signal strength data and phase shift data (plotted versus ore height h) indicate strong sensitivity to parameter values and highly correlated effects. When using the existing model, it is difficult to obtain solution plots that are everywhere reasonably close to signal strength data behaviour. This difficulty is illustrated in Figure 10, which has been obtained after a hand-search for the best values of the parameters D_0, n, σ_w and ϵ_{rb}, and also guided by indicative values from technical drawings and existing literature on soil properties.

Some of the plots in Figure 10 provide a reasonable match to small h signal strength data, while others give better matches to larger h data points. While the four-layer model is promising in capturing many aspects of the large and small oscillations present in data, it fails to provide a single set of parameter values giving a reasonably good match (especially to signal strength data) over the entire height range. Hence, we seek to improve our four-layer model. We do this by considering the effects of scattering off the rough surface of the ore and the effects of belt sag.

Note that the model results for signal strength in Figure 10 indicate a problem with nonuniqueness. There are places where the model is not invertible. That is, a unique value of moisture content cannot be found from the signal strength data, in some ranges of ore height, as evidenced by the crossing-over of model solution curves.

The model results for phase shift do not suffer from this problem; they are nonlinear, but are invertible giving a unique moisture content for a data point $(h, \Delta\phi)$.

4. Extended four-layer model

Before further investigation of the four-layer model's sensitivity to parameter values, we extend the model by allowing for the effects of scattering in a simple way. Scattering is inherently a two- or three-dimensional phenomenon, with waves incident on the rough upper surface of the ore being scattered in various directions.

One consequence is that some of the waves escape to free space without again meeting the receiving antenna, reducing the received signal strength.

The surface of the bauxite ore has been modelled as a level smooth surface that is normal to the direction of microwave travel. This has allowed the use of a model that has a single spatial dimension. In reality, the surface of the ore is lumpy and a little curved, with lump sizes ranging from 12 to 30 mm in diameter. The wavelength in air of our microwaves is approximately 330 mm. This puts the scattering from lumps at this interface in the upper region of the Rayleigh scattering regime where the wavelength is much greater than the roughness length-scale [38].

The effect of the roughness is to scatter microwaves, as they exit the bauxite ore into Region 3 in Figure 2 and as they reflect back upwards from the ore surface after going downwards towards it. There is an entire field of mathematical physics devoted to the study of scattering at interfaces, for example, [38].

The effect of the scattering is to dissipate some of the microwave power out to the environment, undetected by the receiving antenna. Scattering is properly captured by going to a model that is fully three-dimensional, but we seek to imitate some of the consequences of scattering by modifying our four-layer model, by adding attenuation in Region 3, while retaining the simplicity of a one-dimensional model (in space).

The transmitting and receiving antennae are squares with sides $L \approx 0.5$ m, as illustrated in the sketch in Figure 1. The distance from the surface of the ore to the receiving antenna is $D - h$. This distance varies, from approximately $L = 0.5$ m when the belt is empty to approximately 0.2 m when the belt is fully loaded. The solid angle fraction subtended by the receiving antenna on the shadow of the transmitting antenna at the ore surface varies from order one when this distance is near zero to a value that varies approximately linearly with $D - h$, increasing as $D - h$ increases.

A simple over-estimate of an upper limit on losses due to scattering in Region 3 is based on assuming a uniform distribution of energy – the area L^2 of the receiving antenna divided by the total area $L^2 + 4L(D - h)$ of the virtual box of height $D - h$ covering the bauxite provides an estimate of received signal strength SF as a fraction of total signal,

$$SF \approx \frac{L^2}{L^2 + 4L(D - h)}.$$

Here, SF varies from one when $D - h$ is zero to 1/3 when $D - h$ reaches its maximum value $L/2$.

We simulate the loss of signal by introducing a decay term through the value of k in Region 3. Previously, k was the real value valid for propagation through air. We will modify k to $k_3 = k + ik_s$ in Region 3, where $k = \omega\sqrt{\epsilon_0\mu_0} = \omega/c$ is the real value in free space. The value k_s of the imaginary part of k_3 due to scattering will be hand-fitted to get a better model fit to signal strength data. An estimate for k_s is found by requiring the damping term $e^{-k_s(D-h)}$ to equal the upper estimate value of 1/3 when $D - h$ is $L/2$, so that

$$e^{-k_s L/2} = \tfrac{1}{3}.$$

Then using $L = 0.5$ m, our upper estimate is $k_s \approx 4$ m^{-1}. In practice, we find a suitable value for $k_s \approx 1.5$ m^{-1} by matching to data and we generally expect scattering losses to be represented by a number that is much less than four.

4.1. Scattering above ore　We seek to modify the four-layer model, to allow the wavenumber k_3 in Region 3 in Figure 2 to be different to k in free space to imitate one effect of scattering at the surface of the bauxite ore by allowing decaying wave amplitudes in the direction of travel in this region. The augmented matrix (A.8) in Appendix A that summarises the continuity conditions at the three interfaces is then modified to

$$
\left(
\begin{array}{cccccc|c}
1, & 1, & -Z_0, & 0, & 0, & 0 & -Z_0 \\
1, & -1, & Z_b, & 0, & 0, & 0 & -Z_b \\
e^{ik_b h}, & -e^{-ik_b h}, & 0, & Z_b e^{ik_3 h}, & Z_b e^{-ik_3 h}, & 0 & 0 \\
e^{ik_b h}, & e^{-ik_b h}, & 0, & Z_3 e^{ik_3 h}, & -Z_3 e^{-ik_3 h}, & 0 & 0 \\
0, & 0, & 0, & Z_a e^{ik_3 D}, & Z_a e^{-ik_3 D}, & 1 & 0 \\
0, & 0, & 0, & Z_3 e^{ik_3 D}, & -Z_3 e^{-ik_3 D}, & 1 & 0
\end{array}
\right),
$$

where $Z_3 = \mu_0 \omega / k_3$ is the new impedance of Region 3. A series of row reductions leads to an upper triangular augmented matrix that allows to solve for the unknowns,

$$
\left(
\begin{array}{cccccc|c}
1, & 0, & (Z_b - Z_0)/2, & 0, & 0, & 0 & -(Z_0 + Z_b)/2 \\
0, & 1, & -(Z_b + Z_0)/2, & 0, & 0, & 0 & (Z_b - Z_0)/2 \\
0, & 0, & (Z_b + Z_0)e^{-ikh}, & (Z_0 - Z_b)e^{ikh}, & -(Z_0 + Z_b)e^{-ikh}, & 0 & (Z_0 - Z_b)e^{-ik_b h} \\
0, & 0, & 0, & A_s e^{ik_3 h}, & B_s e^{-ik_3 h}, & 0 & C \\
0, & 0, & 0, & 0, & 2Z_3 Z_a e^{-ik_3 D}, & Z_3 - Z_a & 0 \\
0, & 0, & 0, & 0, & 0, & F_s & -2CZ_3 Z_a
\end{array}
\right),
$$

where

$$
F_s = B_s (Z_3 - Z_a) e^{ik_3(D-h)} + A_s (Z_3 + Z_a) e^{-ik_3(D-h)}.
$$

The solution at the receiving antenna with scattering included is given by the last row,

$$
E_{4+}^s(h) = \frac{-2CZ_3 Z_a}{F_s}.
$$

This can be written in the form

$$
E_{4+}^s(h) = \frac{C_2}{(R_1 e^{ik_b h} + R_2 e^{-ik_b h})R_3 e^{ik_3(D-h)} + (R_1 R_2 e^{ik_b h} + e^{-ik_b h})e^{-ik_3(D-h)}},
$$

where

$$
C_2 = \frac{-8Z_0 Z_b Z_3 Z_a}{(Z_0 + Z_b)(Z_b + Z_3)(Z_3 + Z_a)}
$$

and the Fresnel coefficients for each region are

$$
R_1 = \frac{Z_0 - Z_b}{Z_0 + Z_b}, \quad R_2 = \frac{Z_b - Z_3}{Z_b + Z_3}, \quad R_3 = \frac{Z_3 - Z_a}{Z_3 + Z_a}.
$$

Attenuation and phase shift are relative to zero bauxite height values, so we consider the ratio of $E_{4+}^s(h)$ to $E_{4+}^s(0)$, which can be written in the form

$$\frac{E_{4+}^s(h)}{E_{4+}^s(0)} = \frac{(R_1 + R_2)R_3 e^{ik_3 D} + (R_1 R_2 + 1)e^{-ik_3 D}}{(R_1 e^{ik_b h} + R_2 e^{-ik_b h})R_3 e^{ik_3(D-h)} + (R_1 R_2 e^{ik_b h} + e^{-ik_b h})e^{-ik_3(D-h)}}. \tag{4.1}$$

This equation reduces to (2.4) if k_3 is replaced by the free space value k and Z_3 is replaced by Z_0.

Equation (4.1) provides the signal detected at the receiving antenna, normalised on the signal received when no bauxite ore is present. It has a complicated-looking appearance, but consists of terms that are independent of bauxite height h, and terms that depend on bauxite height h through exponentials of $ik_3 h$ and $ik_b h$. These exponentials are multiplied in the denominator of (4.1) to produce exponentials that depend on sums and differences $i(k_3 + k_b)h$ and $i(k_3 - k_b)h$. The real parts of $k_3 + k_b$ and $k_3 - k_b$ provide wave numbers that give wavelengths for the oscillations described by (4.1). The imaginary parts provide oscillation amplitudes that decay in the direction of wave motion.

Evaluating k_3 and k_b using (3.5), (3.8) and (3.1), together with the parameter values listed in Table 1, gives the approximate values,

$$k_b \approx 51 + 2.7i, \quad k_3 \approx 19 + 1.5i,$$

and for the Fresnel coefficients,

$$R_1 \approx 0.5 + 0.02i, \quad R_2 \approx -0.5 + 0.01i, \quad R_3 \approx 1 + 0.04i.$$

The real parts of the sums and differences are

$$\text{Re}(k_3 + k_b) \approx 70, \quad \text{Re}(k_3 - k_b) \approx -30.$$

The resulting wavelengths ($2\pi/k$) for oscillations due to sums and differences of the k are 90 mm and 200 mm. The signal strength according to the four-layer model is

$$SS = 20 \log_{10} \left| \frac{E_{4+}^s(h)}{E_{4+}^s(0)} \right|.$$

Taking the absolute value of a signal that is oscillating about the origin leads to a halving of the apparent wavelength, so that these model results would be consistent with oscillations in signal strength with apparent wavelengths 45 mm and 100 mm. This is broadly in agreement with the signal strength data and model solutions plotted in Figures 10 and 13.

The same wavelengths are visible to a lesser extent in the oscillations in phase shift data and model solutions in Figures 10 and 13. The overall behaviour of the model solution phase shifts is linear in h because it is determined by the term involving the exponential of $i(k_3 - k_b)h$. This term has a modulus that remains larger than the other terms in the denominator of equation (4.1) as h increases, so that adding the other terms modifies it but does not prevent it from winding up in an approximately linear

fashion, to reach a total of ten radians phase shift when h is approximately 0.3 m. This total phase shift is seen in the data and is obtained from the model using the parameter values listed in Table 1.

5. Full results

We now present results from our extended four-layer model, which allows for losses due to scattering of reflected signal off the top of the bauxite ore, and for belt sag. We compare the accuracy of our extension that allows for scattering effects with our previous model which did not allow for scattering. We also investigate the invertibility of data when trying to obtain moisture content from data and we explore the model's sensitivity to parameter values.

5.1. Comparison with previous model In a previous paper [25], there was no scattering in Region 3 of Figure 2. We reproduce that model here by fixing our scattering parameter $k_s = 0$. We compare that previous model with our extended model, by allowing Matlab to automatically minimise the sum of squared residuals between the measured data for signal strength and phase shift and our model results. Allowed ranges and starting values for the parameters that were searched upon are listed in Table 2. For the extended model with scattering, we set the range $k_s \in [0, 4]$ m^{-1} with initial value $k_s = 1.3$, which found the value $k_s = 0.73$ m^{-1}. For the previous model with no scattering, we set the range $k_s \in [0, 0]$. Our extended model with scattering did obtain a fit with a smaller sum of squared residuals (2190) than the previous model (2290), although the extended model did not reach a satisfactory minimum value for the sum of squared residuals during the optimization process.

The resulting fits for the extended model with scattering and for the previous model without scattering are shown in Figures 11 and 12. The extension to approximate the effect of scattering has resulted in a slightly improved fit to the data, as evidenced by the slight reduction in the sum of squares, and by the graphical evidence in Figures 11 and 12 that some of the finer features of the data are better captured by our extended model. The fitted parameters are not much different between the two models. Automated fitting does not provide very convincing fits to the data at typical loading heights near 240 mm, where most of the data are. The curves go nicely through this data region, but do not reproduce very successfully the variation with ore height nearby.

5.2. Invertibility for moisture content An important question that will be addressed in this subsection is whether signal strength and phase shifts are invertible with respect to moisture content, when using the extended four-layer model. The forward problem is solved by our received signal solution (4.1), which provides signal strength and phase shift values, given a variable moisture content and calibrated for the other parameter values affecting the signal. The inverse problem is what needs to be solved when using the microwave analyser to infer moisture content from signal strength and phase shift.

TABLE 2. Model parameters used in an automated search for optimal model fits: initial values used and ranges allowed in minimising the sum of squared residuals between four-layer model solutions and analyser data. The last two columns of numbers are the optimal values found, without scattering and with scattering.

Parameter	Lower bound	Value	Upper bound	No scatter	Scatter	Units
D_0	0.55	0.615	0.65	0.613	0.614	m
S_e	0.05	0.1	0.30	0.05	0.053	m
S_m	0	0.040	0.120	0.090	0.083	m
h_m	0.050	0.200	0.200	0.200	0.169	m
ϵ_{rb}	2	6	15	4.56	4.58	
σ_w	0	1.2	3	1.38	1.66	$S.m^{-1}$
M	0.03	0.1	0.15	0.108	0.096	
n	0.30	0.42	0.60	0.49	0.43	
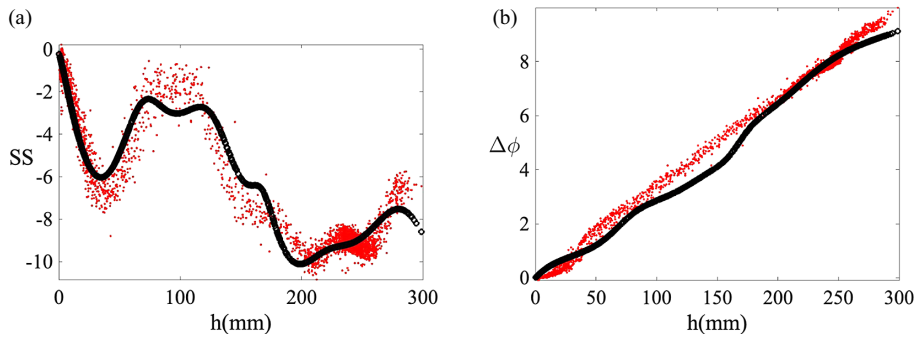
FIGURE 11. Optimal extended four-layer model solution (circles) obtained by fitting automatically to data (dots) by minimising the sum of squared residuals. The model signal strength SS is in dB. The data SS are in arbitrary units and have been linearly scaled to match model SS in dB as part of the optimisation process. Fitted parameter values are listed in Table 2. Scattering in Region 3 is also searched upon by adjusting the parameter k_s.
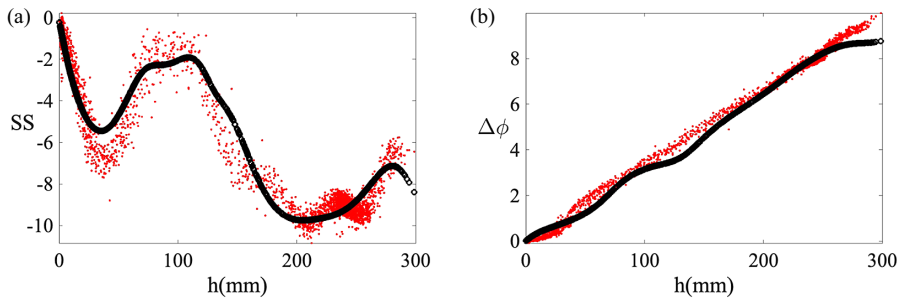

FIGURE 12. Optimal previous four-layer model solution (circles) obtained by setting scattering to zero, fitted automatically to data (dots) by minimising the sum of squared residuals. Details are otherwise as in the caption to Figure 11.
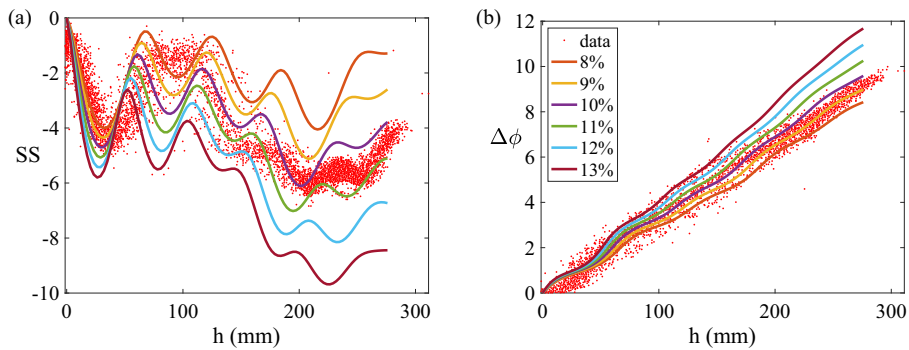
FIGURE 13. Extended four-layer model solutions (lines) compared with data (dot symbols). This model has scattering and sag included. The data are signal strength SS (dB) and phase shift $\Delta\phi$ (radians) at the receiving antenna. The moisture contents M used in the model are listed in the legend. Other parameter values are listed in Table 1. (Colour available online.)

In a previous paper [25], examples were shown where permittivity often could not be inferred solely from signal strength data. This was because there is often no unique solution for permittivity, given signal strength. Another result [25] was that phase shift had very small sensitivity to mixture conductivity. Our Figure 10 indicates that for the un-modified four-layer model, signal strength cannot, in general, be used to uniquely infer moisture content, due to the crossing of lines of constant moisture.

Now that both permittivity and conductivity are given by moisture content through our mixture models, we investigate the extended four-layer model dependence on the single variable M that is moisture content. Also important in the mixture models are the values of D_0, sag, porosity, pure solid bauxite permittivity and pore water conductivity. We fit these values using Maia ship data and acknowledging that different bauxites will likely have different permittivities. Water conductivity depends strongly on dissolved salts and is also expected to vary from shipment to shipment. Zero conductivity is a good assumption for pure bauxite, and water permittivity is well known and does not vary much if dissolved salts are present. Parameter values used for model simulations are listed in Table 1.

Plots equivalent to those in Figure 10, of the extended four-layer model for various moisture contents, are given in Figure 13. Including scattering has largely improved the invertibility of the signal strength data. There remain issues with noninvertibility in some smaller h ranges, especially near $h = 50$ mm and 100 mm. However, at the usual load values with h values above 200 mm, signal strength data are now invertible, potentially providing unique moisture values. Phase data remain invertible – unique moisture values are, in principle, determined by data points.

Independent laboratory measurements, taken on the day the data in Figure 13 were recorded, indicate that moisture content was typically approximately 10% (wet basis) and varied by approximately ±1%. This guided the hand-fitting process that we used
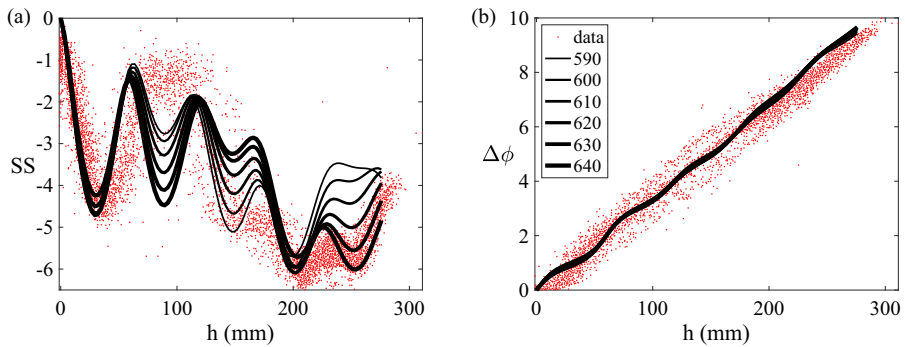
FIGURE 14. Extended four-layer model solutions (lines) compared with data (dot symbols) for various D_0 values. The data are signal strength SS (dB) and phase shift $\Delta\phi$ (radians) at the receiving antenna. The values of D_0 used for each line are given in the legend in mm. Other parameter values are listed in Table 1.

to obtain the parameter values listed in Table 1 and used to obtain the model solutions in Figure 13.

The model solutions give signal strengths in Figure 13 that are highly sensitive to moisture content. The match to signal strength data in that figure suggests that during the day that the microwave and laboratory data were gathered, moisture content varied in the range of 10–11%, assuming that other mixture properties like porosity, solid material permittivity and water purity do not change during the day. The match is not perfect and the phase shift data match indicates a slightly different moisture range of 8–10%.

5.3. Sensitivity to parameters We investigate the sensitivity of our extended four-layer model solution (4.1) to values of the distance D_0, sag, scattering, solid bauxite relative permittivity ϵ_{rb}, pore water conductivity σ_w and porosity n. Note that signal strength data are output in arbitrary units by the microwave analyser. In the following plots, these data have been rescaled for a visual match to solutions to our extended four-layer model, which are in dB.

5.3.1. Spacing D_0 It is clear from Figure 14 that signal strength data are very sensitive to changes in the distance D_0 from the empty conveyor belt to the receiving antenna. Phase shift data are barely affected at the resolutions plotted. If signal strength data are to be used, accurate field measurement of D_0 is essential.

5.3.2. Sag The effects on model solutions of changing the belt sag amplitude term S_m may be seen in Figure 15. Both phase shift and signal strength have visible and significant changes at ore heights above 150 mm, for a sag difference of just 20 mm. Field measurements of belt sag would help eliminate this source of uncertainty in the model.
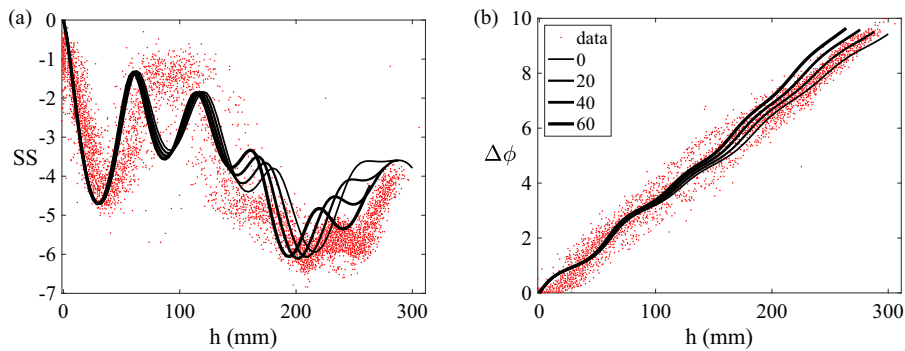
FIGURE 15. Extended four-layer model solutions (lines) compared with data (dot symbols) for various sag S_m values. The data are signal strength SS (dB) and phase shift $\Delta\phi$ (radians) at the receiving antenna. The values of S_m used to compute the sag for each line are given in the legend in mm. Other parameter values are listed in Table 1.
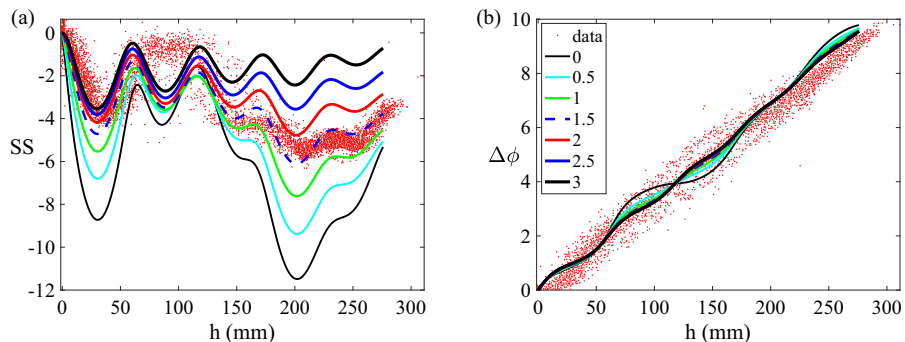

FIGURE 16. Extended four-layer model solutions for various scattering values. Signal strength SS (dB) and phase shift $\Delta\phi$ (radians) are plotted against apparent bauxite height. Data are represented by dot symbols. The values of k_s used for each line for model solutions are given in the legend with units m^{-1}. Other parameter values are listed in Table 1. (Colour available online.)

5.3.3. Scattering Plots showing the effects of scattering on the extended four-layer model solutions can be found in Figure 16. Data have been included, although the scattering data rescaling is arbitrarily chosen to plot near the middle of the model results. There are large amplitude oscillations in signal strength visible when the damping effect k_s from scattering in Region 3 is set to zero. These damp out as k_s increases towards 3 m^{-1}, leaving behind just the oscillations that are due to reflections inside the bauxite ore layer in Region 2. These oscillations are smaller in amplitude and in wavelength than the oscillations due to reflections in Region 3. The effects of changing scattering values on phase shifts are much smaller. This set of plots is useful for understanding the effects of the two sources of oscillations in the solution, the bigger effect from reflections and (constructive and destructive) interference within Region 3, and the smaller effect from reflections and interference within Region 2.
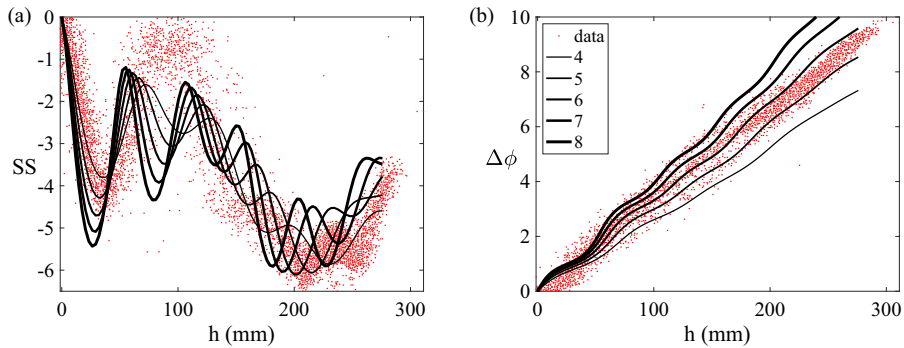
FIGURE 17. Extended four-layer model solutions (lines) compared with data (dot symbols) for various values of solid bauxite relative permittivity ϵ_{rb}. The data are signal strength SS (dB) and phase shift $\Delta\phi$ (radians) at the receiving antenna. The values of ϵ_{rb} used for each line are given in the legend. Other parameter values are listed in Table 1.

Region 3 variations in extent have a bigger effect on signal strength because there is less damping effect in air (due to scattering) in Region 3 than within the bauxite in Region 2.

5.3.4. Bauxite permittivity The calibration of values of solid bauxite permittivity ϵ_{rb} is informed by the plots in Figure 17, where signal strength and phase shifts for the extended four-layer model are plotted against the apparent height h, and compared with data. The phase shift data provide good calibration information, in part because it is in radians and there is no rescaling required. However, the signal strength gives multiple values of solid permittivity for each single data point for most of the data range and is not invertible – in general, it is difficult to infer permittivity from a single signal strength data point. However, the entire graph of signal strength data against bauxite height does provide some guidance for choosing ϵ_{rb}.

5.3.5. Water conductivity The electrical conductivity σ_w is varied in the plots shown in Figure 18 and model results are compared to data. The effect on phase shifts is negligible, while the effect on signal strength is significant. When $\sigma_w = 0$, there is no attenuation in the bauxite and signal strength oscillates about a mean value that increases slightly with ore height. This possibly surprising increase is due to the net effect of the ore providing a better impedance match to the transmitted wave at the receiving antenna.

5.3.6. Ore porosity The extended four-layer model is seen to be very sensitive to the value of porosity n used for fixed moisture content $M = 0.1$ in Figure 19, in both signal strength and phase shift. Since moisture content is fixed, the sensitivity is due to the diluting effect of having more air inside the ore as porosity increases, giving smaller phase shifts and smaller reductions in signal strength.
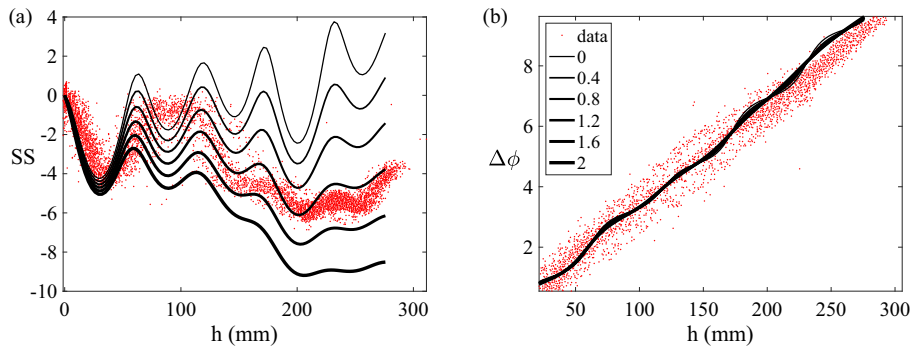
FIGURE 18. Extended four-layer model solutions (lines) compared with data (dot symbols) for various values of water conductivity. The values of water conductivity σ_w used for each line are given in the legend in S.m^{-1}. Other parameter values are listed in Table 1.
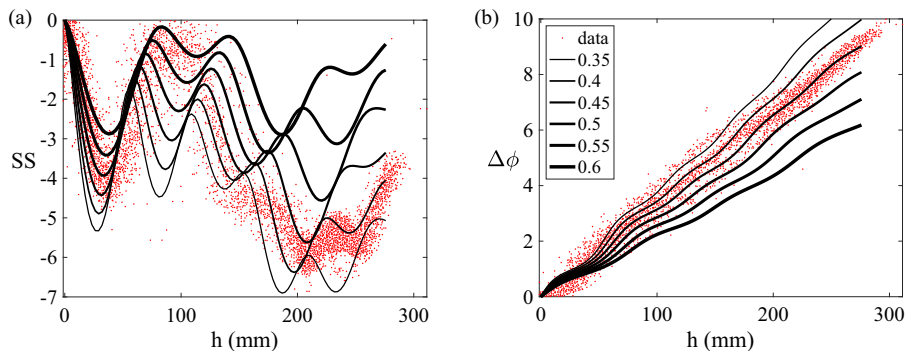

FIGURE 19. Extended four-layer model solutions (lines) compared with data (dot symbols) for various values of ore porosity n. The values of ore porosity n used for each line are given in the legend as volume fractions. Other parameter values are listed in Table 1.

5.3.7. Discussion of sensitivity and fit The model is still challenged to accurately fit the signal strength behaviour versus ore height. Fits that match well for smaller heights require different parameter values to fits that match at larger heights. The four-layer model with scattering provides fits that appear better than without scattering.

The data with which we are comparing has been collected during one day of loading, and is subject to natural variations in moisture content as well as possibly random instrumental errors and variability in physical parameters like porosity and solid permittivity with time. The sensitivity of our model to moisture content exhibited in Figure 13 suggests that moisture content only varies by up to $\pm 1\%$ during one day, which is consistent with laboratory measurements taken during that day that gave actual moisture values in the range $[9, 11]\%$. The high sensitivity seen in Figures 14 and 15 to the distance between the bauxite and the upper antenna, as seen in D_0 and

sag values, means it is important to accurately measure this distance and its variability to an accuracy of millimetres rather than centimetres.

Changes in solid ore relative permittivity have significant effects on both signal strength and phase shift, with changes of order one corresponding to the scatter seen at typical operating ore heights in Figure 17. This sensitivity to the permittivity of the parent ore indicates the importance of regular re-calibration, with significant changes to the data expected if the source of the ore changes, for example, from shipload to shipload. Another option is to investigate how this parameter (solid ore permittivity) varies with source, perhaps in a study conducted alongside of the factory operations over a period of time. The salinity of the water in the ore is also poorly known and can be seen in Figure 18 to have a strong effect on signal strength but negligible effect on phase shift. In the absence of a good prior knowledge of the conductivity of pore water, regular re-calibration will be important if signal strengths are to be included in the microwave analyser's operational inference of moisture content. An accuracy of ± 10 mS.m^{-1} in values of pore water electrical conductivity is needed to get correct signal strength values in the model. Ore porosity values are closely related to conductivity, since salty pore water is the most important contributor to mixture conductivity. Figure 19 indicates that accurate values for porosity with an accuracy of ± 0.01 are required, either by calibration or by direct measurements on offloaded ore.

Overall, the nonlinear and strong dependence on ore height seen in data and in model results means that it is important to accurately measure ore height, and to compensate accurately for the offset inherent in the location and timing of the ultrasound height instrument compared with the microwave receiving antenna.

5.4. Microwave frequency   The extended four-layer model provides an explanation for the nonlinear behaviour observed in data obtained when detecting microwaves that have passed through a layer of ore of thickness h. Signal strength is particularly strongly affected by reflections within the bauxite ore and in the air region between ore and receiving antenna. These reflections lead to augmentation and cancellation effects in the received signal.

One possibly helpful adjustment to improve the operations of the microwave analyser is to try changing the wavelength of the microwaves, which directly impacts these interference effects by changing the wavelengths. A lower frequency increases the wavelengths of microwaves in both air and ore, and might be hoped to reduce the amount of change of interference over the height ranges of ore typically encountered (0–300 mm). We show a series of plots in Figure 20 of strength and phase shifts for model solutions with varying moisture content for various choices of microwave operating frequencies that are smaller than used for our data.

An operating frequency of 50 MHz (which is getting low enough to be radio frequency) has a wavelength in air of approximately 6 m. Our model results in Figure 20 suggest that near this frequency, the assumptions of linear dependence on SS/h and $\Delta\phi/h$ will be much better approximations to actual data behaviour.
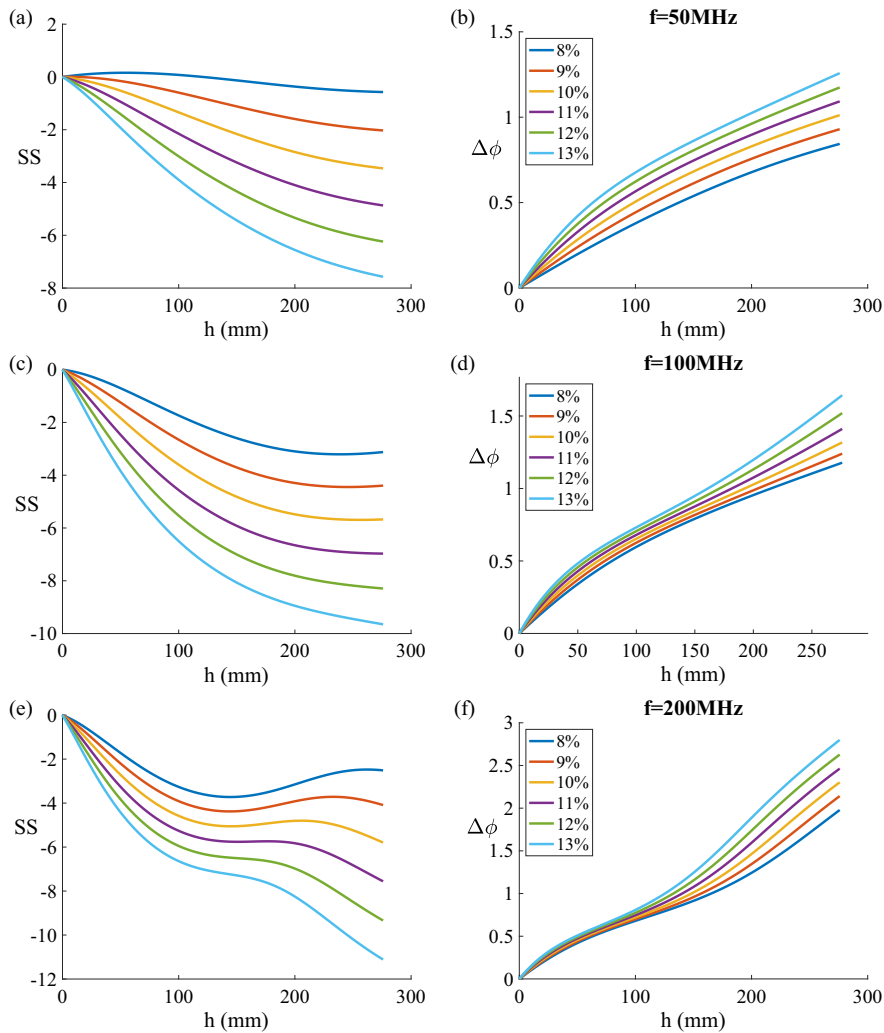
FIGURE 20. Extended four-layer model solutions (lines) for various values of moisture content *M*. Signal frequency has been reduced to 50 MHz, 100 MHz and 200 MHz in the model. Model signal strength SS (dB) and phase shift $\Delta\phi$ (radians) at the receiving antenna are plotted against ore height *h*. The values of moisture content *M* used for each line are given in the legend as %. Other parameter values are listed in Table 1. (Colour available online.)

Higher frequencies lead to more nonlinear behaviour in the signal strength and to less resolution in phase shift data at ore heights below 200 mm.

Using much higher frequencies, in the range of 1–30 GHz, leads to more rapid oscillations in signal strength data that render it unusable for inferring moisture content. It also leads to large phase shifts that might be more difficult to accurately track electronically.

6. Conclusions

An extended four-layer model for microwave propagation through a slab region of bauxite ore has been proposed and solved exactly. The solution successfully matches the main overall characteristics of signal strength and phase shift data obtained from a microwave analyser. Accurate detection of ore moisture content using a standard setup of the analyser has been modelled here and compared with data. The use of signal strength data is not recommended for a linear regression estimate of moisture content at the data operating frequency of 900 MHz, but looks very promising at relatively low frequencies near 50 MHz.

We have sought to improve upon previous modelling work [25] by explicitly linking model results to ore moisture content and by allowing for scattering effects at the top of the ore. Automated fits for both the original and the extended models, as illustrated in Figures 11 and 12, give similar results for moisture content, 9.6% for the extended model and 10.8% for the original model. Both match laboratory results taken during the same time period, where moisture content was measured at various values lying in the range of 9–11%. Automated fitting fails to reproduce the finer details of signal strength behaviour, which are evident however (if not accurately matched) in hand-fitted parameter value sensitivity plots of model solutions.

The modelling we have undertaken, in this paper and in the previous work by Paea et al. [25], is clearly an improvement on the simple linear model that underlies the operation of a microwave analyser. Our results indicate that reflections and the consequent effects of signal augmentation and cancellation largely explain the highly oscillatory behaviour of data. However, it remains true that our extended four-layer model could be further improved to better explain the finer details of signal oscillations seen in the data.

We are focussed here on the forward problem, producing the signal given the moisture content of bauxite ore. The inverse problem remains of interest, the inference of moisture content given a measured signal. The forward modelling reveals and solves for the important role played by multiple reflections within a bauxite ore layer, as well as within the air layer between ore and receiving antenna. These reflections challenge the inverse problem, the interpretation of data to infer moisture content, especially signal strength data. Further work on the practical implications of the four-layer solution for calibrating the microwave analyser, and for using the analyser to infer moisture content in real time while loading ore, is needed. It would be useful to improve upon the current practice when using the analyses of regressing against SS/h and $\Delta\phi/h$, the linear responses consistent with a semi-infinite model.

The model is validated by comparing it to over 20,000 data points collected during one day of operation of a microwave analyser. The model has just six adjustable parameters, so is in no danger of being over-parametrised. Furthermore, the fitting that has been done is simply to narrow down values for these parameters. The physics the modelling is based on, Maxwell's equations and the mixture theory used to relate moisture content to electromagnetic properties, is firmly founded on experimental data and on tested knowledge about electromagnetic wave propagation.

The addition of scattering to our four-layer model was prompted by a desire to improve model fits, and it has improved them even if only slightly. The question of noninvertible signal strength results has also been allayed by adding scattering, as illustrated in Figure 13, where it is clear that a unique moisture content is associated with a given signal strength, provided ore heights are above 100 mm. In any case, any attempt to infer moisture content that uses both signal strength and phase shifts from our model should not suffer from noninvertibility, as the phase shifts resolve any questions about which of several moisture contents to use.

The four-layer model with scattering provides the best fits we have obtained, but the model has taken serious liberties with how it deals with scattering effects. This may be why our model still fails to provide a very accurate match in fine detail to data over the full range of ore heights. A major simplification that remains in our model is that it is one-dimensional in space and that interfaces are normal to the direction of wave propagation. Improvements might include a higher-dimensional treatment of the effects of scattering and curvature at the bauxite ore surface, and allow for the geometry of the conveyor belt and bauxite ore load.

The modelling we have conducted does not consider the possibly important role played by noise in obtaining analyser data. Future modelling with a focus on the inverse problem might profitably investigate the importance of signal-to-noise ratios, especially for very wet ores, as well as the effects of scattering on noise. It would also be useful to investigate the implications of our four-layer model for using data obtained using two different operating frequencies to improve estimates of moisture content.

Appendix A. Four-layer model and solutions

In this Appendix, we summarise the method for solving our four-layer model, for completeness. The description here follows that of Paea et al. [25].

We choose Cartesian axes so that, in Region 1 of Figure 2, $x \leqslant 0$ and the upwards-travelling incident radiation is

$$\mathbf{H}_i = (0, e^{ikx}, 0)e^{-i\omega t},$$
$$\mathbf{E}_i = (0, 0, E_{1+}e^{ikx})e^{-i\omega t},$$

with magnetic field amplitude set to one. Note that the linearity of the equations being solved, and our later normalisation with respect to the solution when $h = 0$, make this amplitude irrelevant. The downwards-travelling reflected wave of unknown amplitude R is

$$\mathbf{H}_r = (0, Re^{-ikx}, 0)e^{-i\omega t},$$
$$\mathbf{E}_r = (0, 0, E_{1-}e^{-ikx})e^{-i\omega t},$$

with

$$E_{1+} = -Z_0,$$

and

$$E_{1-} = RZ_0.$$

The value of E_{1+} follows from setting the upwards-travelling magnetic field amplitude to one, together with Maxwell's equation $\nabla \times \mathbf{E} = -\mu \partial \mathbf{H}/\partial t$ relating electric and magnetic fields. Equation (2.2) becomes

$$k^2 = \omega^2 \epsilon_0 \mu_0 = \frac{\omega^2}{c^2},$$

where $k = 2\pi/\lambda$ is the wavenumber in free space or air and λ is the wavelength in free space. Furthermore, $k = \omega/c = \omega\sqrt{\epsilon_0\mu_0}$, where c is the speed of light. The impedance

$$Z_0 = \mu_0\omega/k = k/(\omega\epsilon_0) = \sqrt{\mu_0/\epsilon_0} \approx 377 \text{ ohms}$$

is a useful combination of parameter values since it appears a number of times.

In Region 2 of Figure 2, where $0 \leqslant x \leqslant h$, the waves are travelling through the bauxite mixture, with fields

$$\mathbf{H} = (0, H(x), 0)e^{-i\omega t}, \quad \mathbf{E} = (0, 0, E(x))e^{-i\omega t},$$

where $E(x)$ in the bauxite can be written in the form

$$E = E_{2+}e^{ik_b x} + E_{2-}e^{-ik_b x}.$$

Equation (2.2) gives

$$k_b^2 = \omega^2 \epsilon_b \mu_b (1 + i\,\mathcal{D}_b), \tag{A.1}$$

where the dissipation is $\mathcal{D}_b = \sigma_b/(\omega\epsilon_b)$ in the bauxite ore mixture. The real part of k_b can be written

$$\text{Re}(k_b) = \omega\sqrt{\frac{\epsilon_b\mu_b}{2}}(\sqrt{1 + \mathcal{D}_b^2} + 1)^{1/2},$$

while the imaginary part is

$$\text{Im}(k_b) = \omega\sqrt{\frac{\epsilon_b\mu_b}{2}}(\sqrt{1 + \mathcal{D}_b^2} - 1)^{1/2}.$$

In Region 3 of Figure 2 where $h \leqslant x \leqslant D$, the radiation travelling upwards from the bauxite is

$$\mathbf{H}_t = (0, T_3 e^{ikx}, 0)e^{-i\omega t}$$
$$\mathbf{E}_t = (0, 0, E_{3+}e^{ikx})e^{-i\omega t},$$

and the travelling wave reflected downwards from the receiving antenna is

$$\mathbf{H}_{r3} = (0, R_3 e^{-ikx}, 0)e^{-i\omega t},$$
$$\mathbf{E}_{r3} = (0, 0, E_{3-}e^{-ikx})e^{-i\omega t}$$

with $E_{3+} = -T_3 Z_0$ and $E_{3-} = R_3 Z_0$.

In Region 4 of Figure 2 where $x \geqslant D$, the receiving antenna is modelled as a semi-infinite material with relatively high electrical conductivity, so that

$$\mathbf{H}_a = (0, H_a(x), 0)e^{-i\omega t},$$
$$\mathbf{E}_a = (0, 0, E_a(x))e^{-i\omega t},$$

and we write the upwards-travelling electric field in the antenna in the form

$$E_a = E_{4+}e^{ik_a(x-D)}.$$

Equation (2.2) gives

$$k_a^2 = \omega^2 \epsilon_a \mu \left(1 + i\frac{\sigma_a}{\omega \epsilon_a}\right).$$

The electromagnetic properties of the receiving antenna are not known to us. The model results are not very sensitive to these parameter values, which are listed in Table 1. Since the root k_a has a positive imaginary part, E_a vanishes as $x \to \infty$.

There are six unknown constants R, E_{2+}, E_{2-}, T_3, R_3 and E_{4+}. Their values are provided by the boundary conditions which give six linear equations that are to be solved simultaneously. The solution we are interested in here is the field amplitude E_{4+} detected at the receiving antenna.

Continuity of E and H at $x = 0$, together with the use of Maxwell's equation

$$\nabla \times \mathbf{E} = -\mu \frac{\partial \mathbf{H}}{\partial t},$$

gives the boundary conditions

$$E_{2+} + E_{2-} - Z_0 R = -Z_0, \tag{A.2}$$

$$E_{2+} - E_{2-} + Z_b R = -Z_b. \tag{A.3}$$

Continuity of E and H at $x = h$ gives the boundary conditions

$$e^{ik_b h}E_{2+} - e^{-ik_b h}E_{2-} + Z_b e^{ikh}T_3 + Z_b e^{-ikh}R_3 = 0, \tag{A.4}$$

$$e^{ik_b h}E_{2+} + e^{-ik_b h}E_{2-} + Z_0 e^{ikh}T_3 - Z_0 e^{-ikh}R_3 = 0. \tag{A.5}$$

Continuity of electric and magnetic tangential fields at $x = D$ gives the boundary conditions

$$Z_a e^{ikD}T_3 + Z_a e^{-ikD}R_3 + E_{4+} = 0, \tag{A.6}$$

$$Z_0 e^{ikD}T_3 - Z_0 e^{-ikD}R_3 + E_{4+} = 0. \tag{A.7}$$

Here, $Z_b = \mu_b \omega / k_b$ is the impedance of the bauxite mixture and $Z_a = \mu_a \omega / k_a$ is the impedance of the receiving antenna.

Then (A.2)–(A.7) can be written in matrix form:

$$\begin{pmatrix} 1, & 1, & -Z_0, & 0, & 0, & 0 \\ 1, & -1, & Z_b, & 0, & 0, & 0 \\ e^{ik_b h}, & -e^{-ik_b h}, & 0, & Z_b e^{ikh}, & Z_b e^{-ikh}, & 0 \\ e^{ik_b h}, & e^{-ik_b h}, & 0, & Z_0 e^{ikh}, & -Z_0 e^{-ikh}, & 0 \\ 0, & 0, & 0, & Z_a e^{ikD}, & Z_a e^{-ikD}, & 1 \\ 0, & 0, & 0, & Z_0 e^{ikD}, & -Z_0 e^{-ikD}, & 1 \end{pmatrix} \begin{pmatrix} E_{2+} \\ E_{2-} \\ R \\ T_3 \\ R_3 \\ E_{4+} \end{pmatrix} = \begin{pmatrix} -Z_0 \\ -Z_b \\ 0 \\ 0 \\ 0 \\ 0 \end{pmatrix},$$

and represented in augmented matrix form as

$$\left(\begin{array}{cccccc|c} 1, & 1, & -Z_0, & 0, & 0, & 0 & -Z_0 \\ 1, & -1, & Z_b, & 0, & 0, & 0 & -Z_b \\ e^{ik_b h}, & -e^{-ik_b h}, & 0, & Z_b e^{ikh}, & Z_b e^{-ikh}, & 0 & 0 \\ e^{ik_b h}, & e^{-ik_b h}, & 0, & Z_0 e^{ikh}, & -Z_0 e^{-ikh}, & 0 & 0 \\ 0, & 0, & 0, & Z_a e^{ikD}, & Z_a e^{-ikD}, & 1 & 0 \\ 0, & 0, & 0, & Z_0 e^{ikD}, & -Z_0 e^{-ikD}, & 1 & 0 \end{array} \right). \tag{A.8}$$

A.1. Four-layer model solution

Row reduction of the augmented matrix (A.8) can be used to write it in upper triangular form, allowing back-substitution to solve for all of the unknown field amplitudes. In particular, the solution for the electric field at the receiving antenna can be written in the form [25]

$$E_a = E_{4+} = \frac{8Z_0^2 Z_a Z_b \ e^{ik(D-h)} e^{ik_b h}}{F},$$

where

$$F = (Z_b^2 - Z_0^2)(Z_0 - Z_a)(e^{2ik_b h} - 1)e^{2ik(D-h)}$$
$$+ [(Z_0 - Z_b)^2 e^{2ik_b h} - (Z_0 + Z_b)^2](Z_0 + Z_a).$$

A.2. Belt sag

We here consider the possibility that as the amount of ore on the conveyor belt increases, the ore weight causes the belt to sag between the rollers that drive it. This is a summary of the approach described by Paea et al. [25]. The microwave analyser is mounted between rollers. Adding belt sag to our model gives a small improvement to fits to signal strength data, by allowing a difference between heavily loaded and lightly loaded conveyor belts. We compute the sag using the formula

$$\text{sag} = \frac{S_m}{\pi} \left[\arctan \left(\frac{h - h_m}{S_e} \right) + \arctan \left(\frac{h_m}{S_e} \right) \right], \tag{A.9}$$

so that sag depends on the true height h of bauxite ore present on the belt. Model matches to data were improved with the choices $S_m = 40$ mm for maximum sag
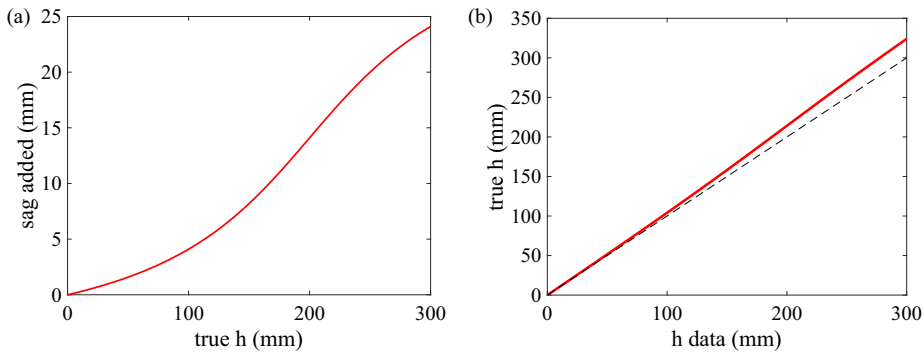
FIGURE 21. Belt sag versus true bauxite height h, and the true bauxite height versus the height measured in strength and phase data. The dashed line in panel (b) shows when true height is equal to data height.

amplitude, $h_m = 200$ mm for the middle of the sag region and $S_e = 100$ mm for the extent of the region over which sagging occurs. These values will be used as default values, unless otherwise stated, in the remainder of this paper. Figure 21 illustrates the dependence of sag on h given by (A.9) and plots the true bauxite height against the height measured in the data. Conversations with an engineer from the bauxite company suggest that belt sag is unlikely to exceed 30 mm.

Data heights are measured using an ultrasound device attached to the upper receiving antenna, pointing downwards to the top of the bauxite layer. Hence, sag will have two effects on the four-layer model. It will increase the distance D from the bottom of the bauxite layer to the receiving antenna, as

$$D = D_0 + \text{sag},$$

and it will make the measured data heights h_m smaller than the true thickness values h, so that

$$h_m = h - \text{sag}.$$

All plots that appear later in this manuscript are against data or apparent h_m values, that is, $h-$sag values are used for plotting model results, to be able to compare them with data.

Acknowledgements

References

[1] L. A. Apresyan, S. I. Rasmagin, V. I. Krasovskiy, V. I. Kryshtob and M. A. Kazaryan, "Basic models of effective parameters for media with complex particles", in: *International conference on atomic and molecular pulsed lasers XIII*, Volume 10614 of *Proc. SPIE* (eds. A. M. Kabanov and V. F. Tarasenko) (SPIE, Bellingham, WA, USA, 2018) 1–8; doi:10.1117/12.2302710.

[2] D. A. G. Bruggeman, "Berechnung verschiedener physicalischer konstanten von heterogenen substanzen", *Ann. Phys.* **5** (1935) 636–679; doi:10.1002/andp.19354160705.

[3] T. L. Chelidze and Y. Gueguen, "Electrical spectroscopy of porous rocks: a review—I. Theoretical models", *Geophys. J. Int.* **137**(1) (1999) 1–15; doi:10.1046/j.1365-246x.1999.00799.x.

[4] T. L. Chelidze, Y. Gueguen and C. Ruffet, "Electrical spectroscopy of porous rocks: a review—II. Experimental results and interpretation", *Geophys. J. Int.* **137** (1999), 16–34; doi:10.1046/j.1365-246x.1999.00800.x.

[5] Y. Chen and D. Or, "Geometrical factors and interfacial processes affecting complex dielectric permittivity of partially saturated porous media", *Water Resour. Res.* **42** (2006) 1–9; doi:10.1029/2005WR004744.

[6] P. R. J. Connolly, M. Josh, K. T. O'Neill, S. J. Seltzer, M. O. Wigand, M. B. Clennell, E. F. May and M. L. Johns, "Dielectric polarization studies in partially saturated shale cores", *J. Geophys. Res. Solid Earth* **124** (2019) 10721–10734; doi:10.1029/2019JB018195.

[7] P. J. De Waal, J. J. Nooteboome and J. P. Poley, "Use of VHF dielectric measurements for borehole formation analysis", *Log Anal.* **19** (1978) 8–30; https://onepetro.org/petrophysics/article-abstract/171679/Use-Of-V-h-f-Dielectric-Measurements-For-Borehole?redirectedFrom=fulltext.

[8] F. J. F. Gonçalves, A. Brancaccio, L. A. Ferreira and E. J. da Silva, "A free-space transmission setup for material parameters estimation with affordable and non-synchronized software-defined radios in the 0.85–1.55 GHz band", *Appl. Sci.* **13** (2023) Article ID: 3010; doi:10.3390/app13053010.

[9] B. I. Halperin and D. J. Bergman, "Heterogeneity and disorder: contributions of Rolf Landauer", *Phys. B* **405** (2010) 2908–2914; doi:10.1016/j.physb.2010.01.002.

[10] T. Hanai, "Dielectric properties of emulsions. III. Dielectric behaviour of water/oil emulsions", *Colloid Polym. Sci.* **177** (1961) 57–61; doi:10.1007/BF01521332.

[11] T. Hanai, *Electrical properties of emulsions in emulsion science* (ed. P. Sherman) (Academic Press, New York, 1968) 354–478; https://lib.ugent.be/catalog/rug01:001669530.

[12] T. Hanai, N. Koizumi and R. Gotoh, "Dielectric properties of emulsions I: dielectric constants of oil/water emulsions", *Colloid Polym. Sci.* **167** (1959) 41–43; doi:10.1007/BF01810121

[13] T. Hanai, N. Koizumi, T. Sugamo and R. Gotoh, "Dielectric properties of emulsions. II. Electrical conductivities of oil/water emulsions", *Colloid Polym. Sci.* **171** (1960) 20–23; doi:10.1007/BF01520319.

[14] A. Hunt, R. Ewing and B. Ghanbarian, *Percolation theory for flow in porous media*, 3rd edn, Volume 880 of *Lect. Notes in Phys.* (Springer, Switzerland, 2014); doi:10.1007/978-3-319-03771-4.

[15] A. G. Hunt, "Basic transport properties in natural porous media: continuum percolation theory and fractal model", *Complexity* **10** (2005) 22–37; doi:10.1002/cplx.20067.

[16] R. Jansson and H. Arwin, "Selection of the physically correct solution in the n-media Bruggeman effective medium approximation", *Opt. Commun.* **106** (1994) 133–138; doi:10.1016/0030-4018(94)90309-3.

[17] A. M. Jayannavar and N. Kumar, "Generalization of Bruggeman's unsymmetrical effective-medium theory to a three-component composite", *Phys. Rev. B* **44** (1991) 12014–12015; doi:10.1103/PhysRevB.44.12014.

[18] R. J. Knight et al., "An introduction to rock physics principles for near-surface geophysics", in: *Near-surface geophysics* (ed. D. K. Butler) (Society of Exploration Geophysicists, Houston, TX, USA, 2005) 31–87; doi:10.1190/1.9781560801719.ch3.

[19] V. I. Kolesnikov, V. B. Yakovlev, V. V. Bardushkin, I. V. Lavrov, A. P. Sychev and E. N. Yakovlev, "Association of evaluation methods of the effective permittivity of heterogeneous media on the basis of a generalized singular approximation", *Dokl. Phys.* **58** (2013) 27–31; doi:10.1134/S1028335813090012.

[20] R. Landauer, "The electrical resistance of binary metallic mixtures", *J. Appl. Phys.* **23** (1952) 779–784; doi:10.1063/1.1702301.

[21] R. Landauer, "Electrical conductivity in inhomogeneous media", in: *Electrical transport and optical properties of inhomogeneous media*, Volume 40 of *AIP Conf. Proc.* (eds. J. C. Garland and D. B. Tanner) (AIP, New York, 1978) 2–45; doi:10.1063/1.31150.

[22] P. Lorrain, D. R. Corson and F. Lorrain, *Electromagnetic fields and waves*, 3rd edn (WH Freeman and Co, New York, USA, 1988); https://eduguidehome.files.wordpress.com/2019/03/electromagnetic-fields-and-waves-by-paul-lorrain.pdf.

[23] M. McGuinness, S. Bohun, V. Cregan, W. T. Lee, J. Dewynne, G. O'Keeffe and T. Vo, "Measuring moisture in bauxite with microwaves", in: *Proceedings of the forum "math-for-industry" 2019 — Mathematics for the primary industries and the environment*, Volume 36 of *Math. Ind.* (eds. R. McKibbin, G. Wake and O. Saeki) (Springer Nature, Singapore, 2021) 13–64; doi:10.1007/978-981-19-1154-5.

[24] J. R. Nimmo, "Porosity and pore-size distribution", in: *Encyclopedia of soils in the environment* (ed. D. Hillel) (Elsevier, London, 2004), 295–303; https://wwwrcamnl.wr.usgs.gov/uzf/abs˙pubs/papers/nimmo.04.encyc.por.ese.pdf.

[25] L. I. Paea, S. Paea and M. J. McGuinness, "Modelling microwaves in bauxite", *ANZIAM J.* **65** (2023), 111–134; doi: 10.1017/S144618112300007X.

[26] C. Pecharromán and J. E. Iglesias, "Effective dielectric properties of packed mixtures of insulator particles", *Phys. Rev. B* **49**(11) (1994) 7137–7147; doi:10.1103/PhysRevB.49.7137.

[27] W. D. Reynolds, B. T. Bowman, C. F. Drury, C. S. Tan and X. Lu, "Indicators of good soil physical quality: density and storage parameters", *Geoderma* **110**(1) (2002), 131–146; doi:10.1016/S0016-7061(02)00228-8.

[28] J. H. Schön, "Chapter 8—Electrical properties", in: *Physical properties of rocks*, Volume 65 of *Dev. Petroleum Sci.* (ed. J. H. Schön) (Elsevier, Amsterdam, The Netherlands, 2015) 301–367; doi:10.1016/B978-0-08-100404-3.00008-1.

[29] J. M. Serrano, S. Shahidian and J. Marques da Silva, "Spatial variability and temporal stability of apparent soil electrical conductivity in a Mediterranean pasture", *Precis. Agric.* **18** (2017) 245–263; doi:10.1007/s11119-016-9460-y.

[30] J. M. Serrano, S. Shahidian and J. R. Marques da Silva, "Apparent electrical conductivity in dry versus wet soil conditions in a shallow soil", *Precis. Agric.* **14** (2013) 99–114; doi:10.1007/s11119-012-9281-6.

[31] A. Sihvola, *Electromagnetic mixing formulas and applications*, Volume 47 of *IET Electromagn. Waves* (The Institution of Engineering and Technology, London, UK, 1999); doi:10.1049/PBEW047E.

[32] A. Sihvola, "Mixing rules with complex dielectric coefficients", *Subsurface Sens. Technol. Appl.* **1**(4) (2000) 393–415; doi:10.1023/A:1026511515005.

[33] R. E. Smith, K. R. J. Smettem, P. Broadbridge and D. A. Woolhiser, *Infiltration theory for hydrologic applications*, Volume 15 of *AGU Water Resources Monogr.* (American Geophysical Union, WA, USA, 2002); doi:10.1029/WM015.

[34] D. Stroud, "The effective medium approximations: some recent developments", *Superlattices Microstructures* **23** (1998) 567–573; doi:10.1006/spmi.1997.0524.

[35] R. H. Tyler, T. P. Boyer, T. Minami, M. M. Zweng and J. R. Reagan, "Electrical conductivity of the global ocean", *Earth Planets Space* **69** (2017) Article ID 156; doi:10.1186/s40623-017-0739-7.

[36]   S. A. A. Vianna, *Microwave-based moisture measurement of bauxite ore on a conveyor belt* (Engineering and Mining Journal: Features, Jan 2013); https://www.e-mj.com/features/microwave-based-moisture-measurement-of-bauxite-ore-on-conveyor-belts/.

[37]   L. Vojtech, M. Neruda and J. Hajek, "Planar material electromagnetic shielding efficiency derivation", *Int. J. Commun. Antenna Propagat.* **1**(1) (2011) 21–28; https://www.researchgate.net/publication/297338460_Planar_materials_electromagnetic_shielding_efficiency_derivation.

[38]   A. G. Voronovich, *Wave scattering from rough surfaces*, 2nd edn (Springer, Berlin–Heidelberg, 1999); doi:10.1007/978-3-642-59936-1.

[39]   Y. Wang, S. Lu, T. Ren and B. Lu, "Bound water content of air-dry soils measured by thermal analysis", *Soil Sci. Soc. Amer. J.* **75** (2011) 481–487; doi:10.2136/sssaj2010.0065.